A&A 510, A22 (2010)
DOI: 10.1051/0004-6361/200913120

Astronomy & Astrophysics

The chemical composition of the Orion star forming region

I. Homogeneity of O and Si abundances in B-type stars⋆,⋆⋆

S. Simón-Díaz[1,2]

[1] Instituto de Astrofísica de Canarias, 38200 La Laguna, Tenerife, Spain
e-mail: ssimon@iac.es
[2] Departamento de Astrofísica, Universidad de La Laguna, 38205 La Laguna, Tenerife, Spain

Received 14 August 2009 / Accepted 27 October 2009

ABSTRACT

Context. Recent accurate abundance analyses of B-type main sequence stars in the solar vicinity has shown that abundances derived from these stellar objects are more homogeneous and metal-rich than previously thought.
Aims. We investigate whether the inhomogeneity of abundances previously found in B-type stars in the Ori OB1 association is real (hence a signature of enrichment of the newly formed stars in an induced star formation scenario) or a consequence of intrinsic errors induced by the use of photometric indices to establish the stellar parameters prior to the abundance analysis.
Methods. We obtained a new (improved) spectroscopic data set comprising 13 B-type stars in the various Ori OB1 associations, and performed a detailed, self-consistent spectroscopic abundance analysis by means of the modern stellar atmosphere code FASTWIND.
Results. We detect systematic errors in the stellar parameters determined previously which affect the derived abundances. Once these errors are accounted for, we find a high degree of homogeneity in the O and Si abundances for stars in the four Ori OB1 subgroups. The derived abundances are in very good agreement with recent determinations in other B-type stars in the solar vicinity. We also compare our results with those obtained for the Sun during the epoch of the "solar crisis", and the Orion nebula.

Key words. stars: early-type – stars: atmospheres – stars: fundamental parameters – stars: abundances

1. Introduction

For many years, our knowledge about the chemical composition of early-B main sequence stars in the solar vicinity has been characterized by two main results: (i) the derived abundances seemed to be highly inhomogeneous (with a dispersion of up to 0.5 dex); and (ii) the mean values indicated lower abundances than the standard (Grevesse & Sauval 1998) set of solar abundances (see reviews by Herrero & Lennon 2004; Morel 2009). These results were not very encouraging, because the inhomogeneity of stellar abundances contradicted with the homogeneity in oxygen abundance found from studying the local diffuse interstellar medium (e.g. Meyer et al. 1998; Cartledge et al. 2006). On the other hand, chemical evolution models of the Galaxy (e.g. Chiappini et al. 2003; Carigi et al. 2005) predict a small enrichment of the ISM in metals during the lifetime of the Sun (i.e. because they are younger than the Sun, nearby OB-type stars are expected to be slightly metal-rich).

Some recent results have began to change this situation. The solar oxygen abundance traditionally considered as a cosmic abundance reference (Grevesse & Sauval 1998) was reviewed by Asplund et al. (2004), who obtained log (O/H) = 8.66 dex, 0.17 dex lower than the standard value. This was the beginning of what has been called the epoch of the"solar crisis": between 2004 and 2008, several studies by different authors (Ayres et al. 2006; Socas-Navarro & Norton 2007; Allende Prieto 2008; Caffau et al. 2008; Ayres 2008; Meléndez & Asplund 2008; Centeno & Socas-Navarro 2008) presented solar oxygen abundances derived by means of different approaches. The calculated values range from 8.63 dex (Socas-Navarro & Norton 2007) to 8.86 dex (Centeno & Socas-Navarro 2008). The debate about its actual value is still open.

Przybilla et al. (2008) have recently analyzed a representative sample of six unevolved early B-type stars in nearby OB associations and the field, and found a very narrow distribution of abundances, with mean values that are more metal-rich compared to previous works (e.g. log (O/H) = 8.76 dex, a value that is within the range of solar abundances calculated during the "solar crisis"). These authors indicate the importance of properly determining the atmospheric parameters and using robust model atoms to avoid systematic errors in the abundance determination. (See also Nieva & Przybilla 2009, for a summary of the main sources of systematic errors affecting the abundance analyses of B-type stars.) The study by Przybilla et al. show that the chemical inhomogeneity previously found for B-type stars in the solar vicinity may be spurious and an artificial effect of those systematic errors. It also reinforces the importance of self-consistent spectroscopic abundance analyses (i.e., the stellar parameters and the metal abundances are determined exclusively from spectroscopic diagnostics by using the same set of stellar atmosphere models). Less accurate photometric $T_{\rm eff}$ estimates must be handle with care (or better avoided whenever

⋆ Based on observations made with the Nordic Optical Telescope, operated jointly on the island of La Palma by Denmark, Finland, Iceland, Norway, and Sweden, in the Spanish Observatorio del Roque de los Muchachos of the Instituto de Astrofisica de Canarias.
⋆⋆ Tables 5 to 18, and Fig. 8 are available in electronic form at http://www.aanda.org

possible!) in the abundance analysis of B-type stars (see also Nieva & Przybilla 2008).

The Orion complex, containing the Orion molecular cloud and the Orion OB1 (Ori OB1) association, is one of the most massive active star-forming regions in the 1 kpc centered on the Sun. Blaauw (1964) divided Ori OB1 into four subgroups of stars – namely Ia, Ib, Ic, and Id – having different locations in the sky and ages. Brown et al. (1994) derived mean ages of 11.4 ± 1.9, 1.7 ± 1.1[1], 4.6 ± 2, and <1 Myr for subgroups Ia to Id, respectively. The youngest subgroup Ori OB1 Id is associated with the Orion nebula (M 42), the most studied H II region and the closest ionized nebula to the Sun in which a high accuracy abundance analysis can be performed.

The correlation between the ages of the stellar subgroups, their location, and the large scale structures in the interstellar medium around Orion OB1 have been interpreted as features of sequential star formation and type-II supernovae (Reynolds & Ogden 1979; Cowie et al. 1979; Brown et al. 1994). Cunha & Lambert (1992, 1994) obtained C, N, O, Si, and Fe abundances of 18 B-type main sequence stars from the four subgroups comprising the Ori OB1 association. They found a range in oxygen abundances[2] of ~0.4 dex, with the highest values corresponding to the stars in the youngest (Id and some Ic) subgroups. In this case, the inhomogeneity in stellar abundances (mainly oxygen and silicon) seemed to be real and coherent with a scenario of induced star formation in which the new generation of stars are formed from interstellar material contaminated by type-II supernovae ejecta.

The study by Cunha & Lambert was based on a photometric estimation of $T_{\rm eff}$ and the fitting of the Hγ line computed from Kurucz (1979) LTE model atmospheres to the observed one to derive $\log g$. In a more recent work, Simón-Díaz et al. (2006) used one of the new generation of NLTE, line blanketed, model atmosphere codes (FASTWIND, Santolaya-Rey et al. 1997; Puls et al. 2005) and a self-consistent spectroscopic approach to derive the stellar parameters and oxygen abundances for the three B0.5 V stars in Ori OB1d (the youngest and, supposedly, more metal-rich subgroup). The resulting stellar parameters were somewhat different and, more important, the derived abundances were systematically lower than the previous values by Cunha & Lambert (1994) by ~0.2–0.3 dex.

This result motivated us to review the chemical composition of the other B-type stars in Ori OB1 to investigate whether the inhomogeneity of abundances previously found is real or a consequence of intrinsic errors induced by the use of photometric indices to establish the stellar parameters prior to the abundance analysis. To this aim, we obtained a totally new (improved) observational data set and performed a self-consistent abundance analysis of 13 of the stars considered by Cunha & Lambert (1992, 1994).

We used FASTWIND to derive the stellar parameters, oxygen, and silicon abundances. The observational data set is described in Sect. 2. The whole spectroscopic analysis is presented in Sect. 3. Then, we compare our stellar parameters and abundance with results from previous works (Sect. 4). The homogeneity of stellar abundances in Ori OB1 and its comparison with other B-type stars in the solar vicinity determinations, the Sun, and the Orion nebula is discussed in Sect. 5. The main conclusions of this work are summarized in Sect. 6.

Table 1. List of B-type stars from Ori OB1 considered in this study, ordered by spectral type.

HD	HR	Name	SpT	V	Subgroup
HD 36512	HR 1855	ν Ori	B0 V	4.62	Ic
HD 37020	HR 1893	θ^1 Ori A	B0.5 V	6.71	Id
HD 36960	HR 1887		B0.5 V	4.78	Ic
HD 37042		θ^2 Ori B	B0.7 V	6.02	Id
HD 36591	HR 1861		B1 V	5.34	Ib
HD 36959	HR 1886		B1 V	5.67	Ic
HD 35299	HR 1781		B1.5 V	5.69	Ia
HD 37744	HR 1950		B1.5 V	6.22	Ib
HD 36285	HR 1840		B2 V	6.33	Ic
HD 36629			B2 V	7.65	Ic
HD 35039	HR 1765		B2 V	4.72	Ia
HD 36430	HR 1848		B2 V	6.23	Ic
HD 35912	HR 1820		B2 V	6.41	Ia

2. Observational data set

The observations used here were carried out with the FIES cross-dispersed, high-resolution echelle spectrograph attached to the NOT2.5 m telescope at El Roque de los Muchachos observatory on La Palma (Islas Canarias, Spain) on 5–8 November 2008. The medium-resolution mode (R = 46 000, $\delta\lambda$ = 0.03 Å/pix) was selected, and the entire spectral range 3700–7300 Å was covered without gaps in a single fixed setting. A sample of 14 stellar candidates was observed, after being selected from the list of stars in the Ori OB1 association analyzed by Cunha & Lambert (1992, 1994). These are early-B type, non-evolved, stellar objects (B0 V–B2 V) with low projected rotational velocities ($v \sin i \leq 60$ km s^{-1}). The signal-to-noise ratio achieved for all the spectra was always above 250. The list of observed stars is presented in Table 1. Apart from the new set of stars, we re-observed HD 37020 and HD 37042, two of the three B-type stars[3] analyzed in Simón-Díaz et al. (2006).

The spectra were reduced with the FIEStool[4] software in advanced mode. The FIEStool pipeline provided wavelength calibrated, blaze-corrected, order-merged spectra of high quality. These spectra were then normalized with our own developed IDL programs. An example of the FIES@NOT spectra for three of the observed stars is presented in Fig. 1, where the Si II-IV and O II lines used for the abundance analysis are also indicated.

3. Spectroscopic analysis

The analyses were performed following a self-consistent spectroscopic approach with the spherically extended, NLTE, line-blanketed stellar atmosphere code FASTWIND (Santolaya-Rey et al. 1997; Puls et al. 2005). Basically, the stellar parameters were derived by comparing the observed H Balmer line profiles and the ratio of Si III-IV and/or Si II-III line equivalent widths with the output from a grid of FASTWIND models. Whenever

[1] Briceño et al. (2005) determined an age for Ori OB1b ~4–6 Myr by studying its low mass, young stellar population; this value is more consistent with what would be expected from the presence of the evolved blue supergiant ϵ Ori in this subgroup.

[2] Other authors (Gies & Lambert 1992; Kilian 1992; Gummersbach et al. 1998) obtained a similar range in oxygen abundances from the analysis of smaller samples of B-type stars in Orion OB1.

[3] HD 37023 was also re-observed, but it was not included in the analysis because we found in the new spectrum that the star is is actually a binary system (SB2), hence not optimal for an abundance analysis.

[4] http://www.not.iac.es/instruments/fies/fiestool/FIEStool.html

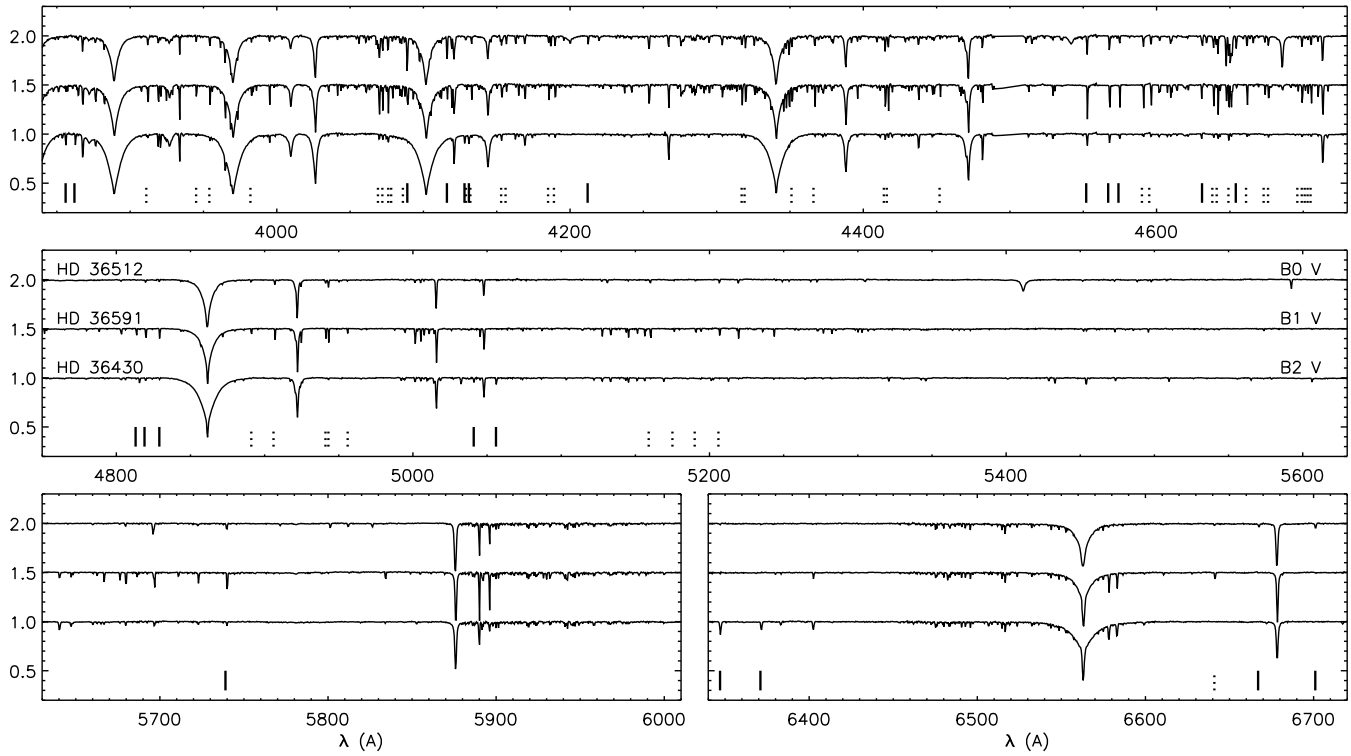

Fig. 1. Example of FIES@NOT spectra for three of the observed stars. The complete atlas is available in the electronic version of the paper (Fig. 8). The Si II-IV and O II lines used for the abundance analysis are indicated as solid and dashed vertical lines, respectively.

possible, the He I-II ionizing equilibrium was also considered. Then, the same grid of models was used to derive the stellar abundances by means of the curve-of-growth method.

3.1. Projected rotational velocities

The projected rotational velocities ($v \sin i$) were obtained by applying the Fourier method (Gray, 1976; see also Simón-Díaz & Herrero, 2007, for its application to OB-type stars) to the Si III λ4552 line. The 0.03 Å/pix resolution of the FIES spectra implies that the lowest $v \sin i$ that could be detected is 2–3 km s^{-1}; however, for those cases with $v \sin i <$ 10–15 km s^{-1}, identifying of the first zero of the Fourier transform was difficult due to the effect of the noise (an maybe the microturbulence).

In many cases, an additional extra Gaussian-type broadening (Θ_g) was needed to properly fit the line profile for the derived value of $v \sin i$. This extra-broadening account for the microturbulence (and maybe the macroturbulence), also affecting the shape of the line. The corresponding derived values are summarized in Table 2.

3.2. Measurement of equivalent widths and identification of problematic lines

The strategy we followed in our analyses is based on the equivalent widths (EW) of metal lines. Therefore, proper identification of the lines of interest, along with an accurate measurement of their EWs (also including the associated uncertainties), is a very important step. We have developed IDL routines automatically identifying metal lines in the spectra, measuring the EWs and their uncertainties, and detecting the possibility that other lines affect these measurements. To this aim we compiled a list of C, N, O, Si, Mg, S, Ne, and Ar lines, extracted from the atomic[5] line list v2.05. For a given line, the program performs a multi-Gaussian fit of the observed line profile accounting for all the lines expected to be present in a certain spectral range ($\lambda_0 \pm 2$ max[$v \sin i \lambda_0$/c, $0.5\lambda_0$/R]) around the wavelength indicated in the line list. The uncertainty in the EW measurement is obtained by assuming the location of the local continuum at $\pm 1/SNR$ and, in those cases in which the line is isolated, comparing the value obtained by means of the Gaussian fitting with the value derived by integrating the line.

The high quality of our spectra allowed us to identify and measure the EWs of up to 27 Si II-IV lines and 47 O II lines. Some of the lines were labeled as problematic because of the presence of one or more lines from other elements (e.g. the O II λ4673.73 line may be affected by the C III λ4673.95 in same cases; similarly occurs for the O II λ4641.81 line, coincident with the N III λ4641.85 line). These lines were treated with special care in the abundance analysis, since they may be giving wrong values for the abundance.

Table 2. Projected rotational velocities derived for the studied stars.

HD	$v \sin i^a$	$\Theta_g{}^a$	HD	$v \sin i$	Θ_g
HD 36512	15	30	HD 37744	37	00
HD 37020	55	00	HD 36285	<10	20
HD 36960	23	40	HD 36629	<10	15
HD 37042	31	00	HD 35039	<12	15
HD 36591	08	19	HD 36430	<15	25
HD 36959	12	12	HD 35912	<12	20
HD 35299	<08	12			

Notes. [(a)] Both quantities in km s^{-1}.

[5] http://www.pa.uky.edu/~peter/newpage/

Table 3. Final results of the HSi analysis: stellar parameters and Si abundances.

Target	SpT	$(EW_4/EW_3)^a$ $T_{\rm eff}$ – Si IV-III	(EW_{2A}/EW_3) $T_{\rm eff}$ – Si II-III	(EW_{2B}/EW_3) $T_{\rm eff}$ – Si II-III	$T_{\rm eff}$ – He I-II	Adopted $T_{\rm eff}$	Adopted $\log g$	ξ_t(Si)	$\epsilon_{\rm Si}\pm\Delta\epsilon_{\rm Si}[\sigma, \xi_t]$	$T_{\rm eff}\pm500$ K $\Delta\epsilon_{\rm Si}$ (Si III)
		(1.42 ± 0.06)								
HD 36512	B0 V	33 700 ± 200	...	...	34 000 ± 500	**33 700**	**4.2**	4.3 ± 0.7	**7.49**± [0.07, 0.05]	±0.12
		(0.69 ± 0.09)								
HD 37020	B0.5 V	30 500 ± 600	...	...	30 000 ± 500	**30 500**	**4.2**	0.5 ± 0.5	**7.47**± [0.10, 0.04]	±0.06
		(0.60 ± 0.04)								
HD 36960	B0.5 V	28 900 ± 300	...	...	29 000 ± 500	**28 900**	**3.9**	5.4 ± 0.6	**7.53**± [0.02, 0.06]	±0.06
		(0.64 ± 0.07)								
HD 37042	B0.7 V	29 700 ± 400	...	...	29 500 ± 500	**29 700**	**4.2**	1.4 ± 0.3	**7.55**± [0.03, 0.04]	±0.05
		(0.39 ± 0.01)								
HD 36591	B1 V	27 200 ± 100	...	...	...	**27200**	**4.1**	1.3 ± 0.3	**7.53**± [0.06, 0.03]	±0.01
		(0.25 ± 0.02)	(0.12 ± 0.02)							
HD 36959	B1 V	25 900 ± 300	25 900 ± 100	...	...	**25 900**	**4.2**	0.0 ± 1.0	**7.50**± [0.05, 0.07]	∓0.02
		(0.16 ± 0.03)	(0.12 ± 0.01)	(0.12 ± 0.04)						
HD 37744	B1.5 V	23 900 ± 600	25 700 ± 100	23 600 ± 600	...	**23 800**	**4.1**	0.5 ± 0.5	**7.54**± [0.06, 0.04]	∓0.05
		(0.14 ± 0.02)	(0.20 ± 0.01)	(0.17 ± 0.03)						
HD 35299	B1.5 V	23 900 ± 300	24 900 ± 300	23 700 ± 300	...	**23 700**	**4.2**	0.5 ± 0.5	**7.50**± [0.08, 0.02]	∓0.06
			(0.26 ± 0.01)	(0.41 ± 0.03)						
HD 36285	B2 V	...	23 900 ± 200	20 600 ± 200	...	**20 600**	**4.0**	1.7 ± 0.5	**7.49**± [0.06, 0.05]	∓0.11
			(0.36 ± 0.02)	(0.44 ± 0.04)						
HD 35039	B2 V	...	22 200 ± 200	19 900 ± 200	...	**19 800**	**3.7**	3.3 ± 1.0	**7.52**± [0.06, 0.08]	∓0.14
			(0.39 ± 0.02)	(0.53 ± 0.02)						
HD 36629	B2 V	...	22 800 ± 300	20 000 ± 100	...	**20 000**	**4.1**	1.0 ± 0.5	**7.54**± [0.04, 0.05]	∓0.13
			(0.65 ± 0.06)	(0.96 ± 0.09)						
HD 36430	B2 V	...	21 000 ± 300	18 600 ± 200	...	**18 600**	**4.1**	3.5 ± 1.0	**7.47**± [0.08, 0.07]	∓0.13
			(0.73 ± 0.05)	(0.92 ± 0.05)						
HD 35912	B2 V	...	20 400 ± 300	18 500 ± 150	...	**18 500**	**4.0**	3.2 ± 0.5	**7.48**± [0.07, 0.04]	∓0.13

Notes. Detailed results (line-by-line) of the Si abundance analysis are presented in Tables 6 to 18. All $T_{\rm eff}$ values correspond to the $\log g$ indicated in the 8th column.
[(a)] EW_4: Si IV 4116; EW_3: Si III 4552; EW_{2A}: Si II 4130; EW_{2B}: Si II 6371.

Generally, the Gaussian fit provides reliable results for the *EW*s; however, in those cases in which the $v \sin i$ of the star is above 30–35 km s^{-1}, the use of a Gaussian to fit the profile may result in an under or overestimation of the *EW* (in a few percent), depending on the line strength. For those cases, the *EW* resulting from the integration of the observed line profile was preferred.

3.3. A grid of HHeOSi FASTWIND models

For this study, we constructed a grid of FASTWIND models with $T_{\rm eff}$ and $\log g$ ranging from 17 to 36 kK (1 kK steps) and 3.7 to 4.3 dex (0.1 dex steps). As the studied stars are not expected to be evolved, the He abundance was fixed to 0.09 dex. In addition, since FASTWIND is a spherically extended code, the radius and other wind parameters need to be indicated, and are grouped in the Q-parameter. We fixed this parameter to $\log Q = -15$ as a representative value for which the wind effect over the optical spectrum is practically negligible. (Hα and He IIλ4686 show no sign of wind contamination.) The metallicity was assumed to be solar (following the set of abundances by Grevesse & Sauval 1998).

For each pair of stellar parameters, a sub grid of models varying the microturbulence ($\xi_t = 1$, 3, 5, 7, 9 km s^{-1}), the Si abundance ($\epsilon_{\rm Si} = -5.10$, –4.80, –4.50, –4.20 dex), and the O abundance ($\epsilon_{\rm O} = -4.00$, –3.65, –3.30, –2.95 dex) was calculated. The O and Si atomic models used for the grid came mainly from Becker & Butler (1988, 1990). However, two updates were considered: (a) a extended Si II model atom (see Trundle et al. 2004), and (b) the most recent log gf values indicated in the atomic line list v2.05 for the formal solution calculations.

The final grid consists of 20×7×4 (=560) models and a total of 2800 formal solutions (5 microturbulence values per model). It includes line profiles and *EW*s for H , He I-II, Si II-IV and O II lines, along with the spectral energy distribution for each set of stellar parameters.

3.4. Determining stellar parameters

The use of the Si III-IV and/or Si II-III ionization equilibrium, along with the H Balmer lines, for determining the stellar parameters of early B-type stars is a longstanding method described elsewhere (see e.g. Kilian et al. 1991; Urbaneja et al. 2005; Crowther et al. 2006; Markova & Puls 2008). The ratios EW(Si IV λ4116)/EW(Si III λ4552) and/or EW(Si II λ4128)/EW(Si III λ4552), depending on the temperature of the star have been traditionally used as $T_{\rm eff}$ indicators. This decision has been probably motivated by the fact that these are the strongest, unblended lines in the spectral range commonly observed for the stellar abundance analysis (i.e. ~4000–5000 Å).

We derived the stellar parameters, along with the Si abundance, for all stars in our sample using this methodology. We initially considered that these Si line ratios determine the effective temperatures (Cols. 3 and 4 in Table 3). However, motivated by a couple of problems found when deriving the stellar parameters in the cooler objects (see discussion below), we decide to include the EW(Si II λ6347)/EW(Si III λ4552) ratio as a temperature indicator (Col. 5). The measured values are indicated in brackets in the corresponding columns. As expected, the Si IV/Si III ratio

decreases when we move to later spectral types, and the Si II/Si III behaves in the opposite way. For three of the stars (HD 36959, HD 35299, and HD 37744), lines from the three ions are clearly and simultaneously present in the spectra.

Four parameters need to be determined at the same time in an iterative way: $T_{\rm eff}$, $\log g$, $\xi_{\rm t}$(Si), and $\epsilon_{\rm Si}$. First, we use the Si line ratios indicated above and the wings of the H Balmer lines (fixing $\xi_{\rm t}$(Si), and $\epsilon_{\rm Si}$) to obtain an initial guess for $T_{\rm eff}$ and $\log g$. Then we apply the curve of growth method to a proper set of Si II-IV lines to iteratively obtain final values for the four parameters (a detailed description of the used lines and the results of the Si abundance analysis is presented below). Normally, the final values of $T_{\rm eff}$ and $\log g$ are quite close to the initial values, since the mentioned line ratios are only slightly dependent on $\epsilon_{\rm Si}$ and $\xi_{\rm t}$.

3.4.1. Hotter objects ($T_{\rm eff} \geq 27\,000$ K)

In the hotter objects, Si II lines are not present in the spectra. The EW(Si IV λ4116)/EW(Si III λ4552) ratio is thus used to obtain the initial guess values of $T_{\rm eff}$ for each of the $\log g$ values considered in the grid. Then, the full set of reliable Si III-IV lines, along with the H Balmer line profiles, is used for fine determination of the four parameters indicated above (see an example in the upper panel of Fig. 2, and in Fig. 3). The uncertainties in the EW measurements of the Si lines have been taken into account for establishing the uncertainties associated with the derived stellar parameters. Generally, the $T_{\rm eff}$ and $\log g$ can be determined with an accuracy better than 500–600 K and 0.1 dex, respectively. The final results of the analysis are presented in Table 3.

For main sequence stars with $T_{\rm eff} \gtrsim 28\,000$ K the He I-II ionization equilibrium can also be used (see e.g. Herrero et al. 1992; Simón-Díaz et al. 2006). (Below this temperature, He II lines are too faint or not present in the spectrum.) We could determine the stellar parameters in this way for four of the stars in our sample. An example of this type of analysis has already been presented in Simón-Díaz et al. (2006), so we only present here the corresponding results (see Col. 6 in Table 3). In general, there is good agreement between the $T_{\rm eff}$ determined through the Si III-IV and the He I-II ionization balance with differences in $T_{\rm eff}$ not larger than ~500 K.

3.4.2. Cooler objects

For the cooler objects, the Si II/Si III must be used. We initially considered the EW(Si II λ4130)/EW(Si III λ4552) ratio for obtaining a first estimation of the stellar parameters; however, we found two facts that warned us of a possible problem with the Si II λ4130 (or the Si II λ4128) line. First, it was not possible to properly fit the H Balmer lines for any of the ($T_{\rm eff}$, $\log g$)-pairs indicated by the Si II λ4130/Si III λ4552 line ratio, because the core of the H synthetic lines were somewhat narrower than the observed ones (even if high values of $\log g$ are considered). For these temperatures, the cores of the H Balmer lines begin to be sensitive to changes in $T_{\rm eff}$. For all the cases studied, these lines require somewhat lower effective temperatures to properly fit their cores. Second, the $\epsilon_{\rm Si}$-EW diagnostic diagrams show two sets of Si II lines giving different abundances by ~0.2 dex (see lower panel in Fig. 2). Curiously, each subset of lines corresponds to transitions with very different energy levels (Si II $\lambda\lambda$4128, 4130, 5041, 5056, in one hand, coming from higher energy levels; Si II $\lambda\lambda$6347, 6371, 3856, 3862, on the other, comming from lower energy levels; we suggest the reader have a Grotrian diagram in hand). This different behavior of the various lines warned us of possible problems with the Si II atomic model and of using Si II λ4128 line alone to establish the stellar temperature.

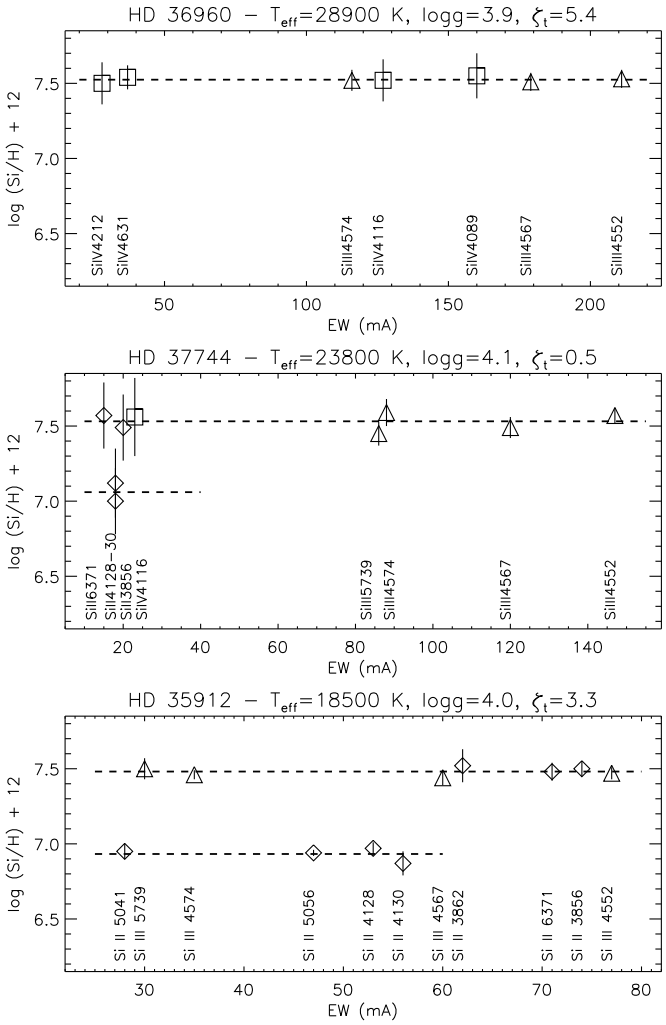

Fig. 2. Silicon abundance vs. EW diagnostic diagrams for three of the analyzed stars (with representative effective temperatures).

Columns 4 and 5 in Table 3 show the different effective temperatures obtained depending on the Si II line that is used (Si II λ4128, Si II λ6371). Temperatures given by the EW(Si II λ6371)/EW(Si III λ4552) ratio are systematically lower by up to ~2000–3000 K. In addition, a proper fit of the cores of the H Balmer lines can be achieved with these new values of the temperature.

3.4.3. HD 36595, HD 37744, and HD 35299

These three stars show Si II-III-IV lines in their spectra, so can contribute with new decisive clues to the problem mentioned above. In this case we count with three $T_{\rm eff}$ indicators. As can be noticed from inspection of Table 3, the $T_{\rm eff}$ indicated by the EW(Si II λ6371)/EW(Si III λ4552) ratio results in better agreement than the other Si II/Si III ratio for two of the three cases. For the hotter object (HD 36959), the Si II λ6371 is too faint to be measured. Although the $T_{\rm eff}$ indicated by the EW(Si II λ4130)/EW(Si III λ4552) ratio agrees with

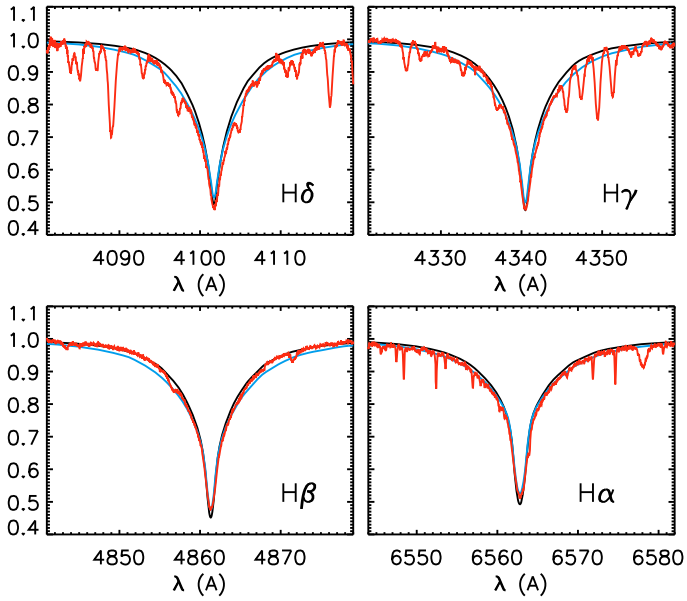

Fig. 3. Example of fitting the H Balmer lines to determine $\log g$. Two FASTWIND models are compared with the observed spectrum (red line) of HD 36960: in black, model with the stellar parameters resulting from the FASTWIND HSi analysis (28 900, 3.9); in blue, model with the stellar parameters derived by Cunha & Lambert (1992), for comparison (28 900, 4.3).

the Si IV/Si III diagnostic in this object, this is not the case for the other objects.

In Fig. 2 (middle panel) we show the $\epsilon_{\rm Si}$-EW diagnostic diagram for HD 37744. The stellar parameters considered in this plot are those indicated by the Si IV/Si III ratio. The Si II $\lambda\lambda$6371, 3856 lines fit the other Si III-IV lines perfectly, but not the Si II $\lambda\lambda$4128, 4130 lines.

3.4.4. Concluding

We found some indications of a problem in the Si II model atom that led to bad modeling of the Si II $\lambda\lambda$4128, 4130, 5041, 5056 lines. Fortunately, our observations also include other Si II lines that seem to behave properly. A review of the Si II model atom is needed (and could be tested with the type of detailed analysis presented here), but in the meantime, several arguments allow us to trust[6] the Si II $\lambda\lambda$6347, 6371, 3856, 3862 set of lines for the stellar parameter determination and for abundance analysis of the cooler objects in our sample: (a) the coherence of results between Si IV-III and Si III-II in terms of $T_{\rm eff}$; (b) the good fit of the H Balmer lines for the cooler stars when the lower $T_{\rm eff}$ is considered; (c) the coherence of results in Si and O abundances that is obtained for all the stars in our sample when this solution is adopted (see below).

3.4.5. Uncertainties

Columns 3 and 5 indicate the uncertainties in $T_{\rm eff}$ obtained from considering errors in the EWs measurement of Si II-IV lines. These uncertainties, obtained by assuming a fixed gravity are ~100–600 K. Gravity can be normally established with an accuracy better 0.1 dex. Uncertainties from both quantities are correlated, e.g. a positive variation of $\log g$ of 0.1 dex needs to be compensated by an increase of $T_{\rm eff}$ ~ 100–300 K to guarantee again the Si ionization balance. Although in many cases the formal errors in temperature obtained from the propagation of EWs errors are smaller than 500 K, our experience warns us to be conservative (since other parameters can also slightly affect the derived temperatures, such as the considered microturbulence). Therefore, we adopt 500 K and 0.1 dex as characteristic uncertainties in $T_{\rm eff}$ and $\log g$, respectively, from our analyses.

[6] This hypothesis is also supported by a comparison of $T_{\rm eff}$ obtained for the cooler objects in our sample from other spectroscopic diagnostic based on O II/I and C III/II ratios of lines (F. Nieva, private communication).

3.5. Silicon and oxygen stellar abundances

We applied the curve-of-growth method to derive Si and O abundances. This method considers a grid of models for a given set of stellar parameters ($T_{\rm eff}$ and $\log g$) in which the microturbulence and the abundance of the element to be studied are varied. An abundance is obtained for the various values of microturbulence for each of the considered lines (given the measured EW of the lines in the observed spectrum). Then, the final abundance is given by that microturbulence that results in all lines giving the same abundance. More details on this method can be found in e.g. Kilian (1992) or Simón-Díaz et al. (2006).

Our preference for this methodology in performing the abundance analysis is that we find the curve-of-growth method very powerful for identifying problematic lines (as shown e.g. in the previous section), which can affect the final abundance determination, and provide precise estimations of the uncertainties associated with the dispersion of line-to-line abundances, microturbulence, and the stellar parameters.

3.5.1. Silicon abundances

As mentioned, silicon abundance is obtained at the same time as to the stellar parameters. Once a first estimation of the stellar parameters was obtained through the EW(Si IV λ4116)/EW(Si III λ4552) and/or EW(Si II λ6371)/EW(Si III λ4552) line ratios, the curve-of-growth method was applied to a proper set of Si lines to derive the Si abundance, together with the final values of the stellar parameters and a microturbulence.

Initially, we included all the measured lines in the analysis, but identified some problematic lines. By *problematic lines* we mean lines giving abundances that are too high or too low compared with the mean value provide by a set of lines initially considered as reliable. These problematic lines were removed in the final analysis. To illustrate the procedure, we consider the case of HD 36960. The $\epsilon_{\rm Si}$-EW diagram with whole set of measured Si lines (Si III and Si IV lines, in this case) is shown in Fig. 4. As the initial set of reliable lines we consider the Si III $\lambda\lambda$4552, 4567, 4574 triplet and the Si IV λ4116 line. The other Si IV lines provide similar abundances to the first set of reliable lines, except Si IV λ6701. The situation is less encouraging for the other Si III lines, since all of them lie below the mean abundance value from reliable lines. We thus label these lines as problematic. The same procedure was followed for the selection of reliable Si II lines (see Sect. 3.4).

A similar behavior is found for the problematic lines in all the analyzed stars. Since the EW of these lines are accurately measured and no lines from other elements are expected to be

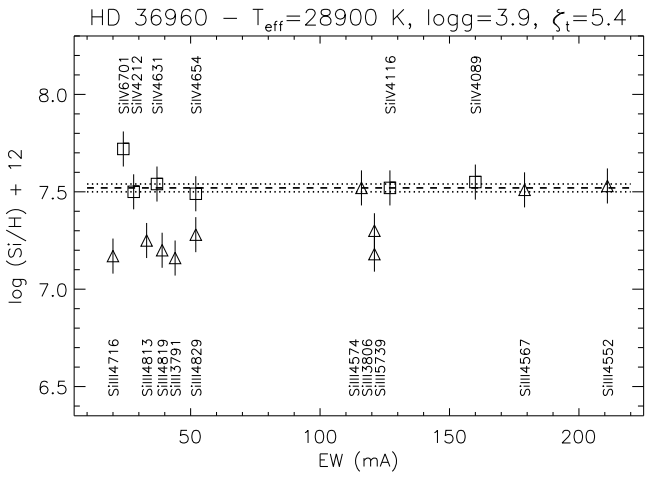

Fig. 4. Silicon abundance vs. *EW* diagnostic diagrams for HD 36960. All the observed Si III-IV lines are included in the plot. Uncertainties in the individual line abundances (propagated from the errors in the measured *EW*s) are indicated as vertical lines.

affecting them[7], we argue that the discrepancy may be related to the definition of the model atom. For example, the Si III $\lambda\lambda$4813, 4819, 4829 triplet is known to give different results than the Si III $\lambda\lambda$4552, 4567, 4574 triplet because of the boundary problems of the Si III model atom (Becker & Butler 1990). Normally, there is an explanation for the bad behavior of the problematic lines; therefore, the exclusion of lines from the analysis is not arbitrary (e.g. lines from the same multiplets behave in the same way and are normally excluded all together).

It is important to notice that the analysis with the whole set of lines (including the problematic ones) could lead to an incorrect determination of the microturbulence, hence of the final value of Si abundance.

Final results of the Si abundance analysis[8] are indicated in Table 3 (Cols. 9 and 10). Three sources of errors must be considered for estimating of the final uncertainty: (1) the dispersion in the line-by-line abundances; (2) the uncertainty associated with the microturbulence, (indicated in Table 3, and Tables 6–18, only available in the electronic version); and (3) the contribution of uncertainties in the stellar parameters. These can be added quadratically to obtain the total uncertainty.

For illustrative purposes in the last column of Table 3, we indicate the effect of a change of ±500 K in $T_{\rm eff}$ on the Si abundance if this was derived exclusively by using Si III lines[9]. The minimum effect occurs for $T_{\rm eff} \sim 27\,000$ K and increases towards higher and lower temperatures (note the change in the sign of the uncertainties), reaching values up to 0.12 dex. This behavior is a consequence of the dependence of the *EW* of the Si III lines with temperature. The maximum *EW* is achieved around 27 000 K (so the abundance is quite insensitive to small changes in $T_{\rm eff}$), and decreases towards lower and higher temperatures (also increasing its sensitivity to $T_{\rm eff}$ variations). When lines from two different ions are used, the final Si abundance can be constrained with better accuracy, since the *EW* of lines from different ions behaves in a opposite way for a given $T_{\rm eff}$. As a consequence in this case, the uncertainty associated with the stellar parameters is always negligible compared with the dispersion in the line-by-line abundances.

3.5.2. Oxygen abundances

Up to 47 O II lines were identified in the observed spectral range. However, not all the lines were finally used for the O abundance determination. The selection of the final set of lines used for the analysis was based on a detailed analysis by multiplets (following similar criteria to the case of Si, but in this case we studied the behavior of lines resulting from different multiplets). We found a similar behavior of lines to the one described in Simón-Díaz et al. (2006).

The derived O abundances are indicated in Table 4, and the results of the line-by-line analyses in Tables 6–18 (in the electronic version). For this element, only lines from one ionization state were available, so we could not test whether the corresponding ionization equilibrium (O III/II or O II/I) is achieved for the considered stellar parameters. We adopt for the oxygen abundance analysis the same stellar parameters as in the Si analysis.

We found (as in many previous works) that the microturbulence derived from the O II lines ($\xi_{\rm t}$(O)) differs from the Si analysis ($\xi_{\rm t}$(Si)), and a somewhat larger microturbulence is derived. Some authors assume the $\xi_{\rm t}$(Si) value (or a mean value of the microturbulences obtained for the various elements analyzed) to perform the oxygen abundance analysis. In our opinion, this can lead to significant systematic errors in the analysis. Since this is an ad-hoc parameter that is still not well understood (see, however, Cantiello et al. 2009), we adopt the microturbulence derived from the oxygen analysis itself, for consistency.

In fact, determination of the microturbulence value that will be adopted in the final steps of the abundance determination is an important task. Unidentified problems in the O II line modeling or bad measurements of the corresponding *EW*s (due to blends, noise, or a bad placement of the continuum) can enormously affect the $\xi_{\rm t}$ value that produces a zero slope in the $\epsilon_{\rm O}$-*EW* diagrams. A detailed analysis by multiplets (see Simón-Díaz 2005) can help identify problematic lines and to better decide on the final microturbulence to be adopted.

Table 4 also indicates the uncertainties associated with errors in the line-to-line abundance dispersion, the microturbulence, and the stellar parameters. In addition, last column shows the derived abundances if the effective temperature is varied ±500 K. (Although the exact values are not shown here, the contribution of the log g uncertainty to the oxygen abundance can be considered negligible in comparison with the $T_{\rm eff}$ contribution.) The derived oxygen abundance is very sensitive to changes in $T_{\rm eff}$ for the cooler and hotter objects, and there is a change in the behavior of the oxygen abundance with $T_{\rm eff}$ around 27 000 K. This behavior is similar to the one illustrated in Table 3.

4. Comparison with previous works

Two of the stars included in this analysis have already been analyzed in Simón-Díaz et al. (2006). These are HD 37020 and HD 37042. We observed the two stars again to have spectra with the same characteristics as the other stars in the sample. The stellar parameters presented in Table 2 correspond to the analysis of the new spectra. The new analysis resulted in slightly higher

[7] This is not the case for Si IV $\lambda\lambda$4089, 4631, and Si II $\lambda\lambda$6347, 3856; these lines may be blended with O II λ4089, N II λ4631, Mg II λ6347, and O IIλ3856, respectively, in some cases. The high resolution of the FIES@NOT spectra normally allows separating both line contributions; however, results with these lines are always treated with care.

[8] Results of the line-by-line analysis are presented in Tables 6–18.

[9] A similar test assuming a change of 0.1 dex in log g indicates negligible effects when compared with the $T_{\rm eff}$ contribution.

Table 4. Final results of the O abundance analysis. Detailed results (line-by-line) of the O abundance analysis are presented in Tables 6 to 18.

Target	SpT	$T_{\rm eff}$	$\log g$	$\xi_{\rm t}$(O)	$\epsilon_{\rm O}$	$\Delta\epsilon_{\rm O}(\sigma)$	$\Delta\epsilon_{\rm O}(\xi_{\rm t})$	$\Delta\epsilon_{\rm O}(T_{\rm eff}\pm500)$	$\epsilon_{\rm O}(T_{\rm eff}+500, T_{\rm eff}-500)$
HD 36512	B0 V	33 700	4.2	4.4 ± 1.5	**8.71**	0.10	0.05	±0.06	(8.76, 8.65)
HD 37020	B0.5 V	30 500	4.2	6.4 ± 1.6	**8.70**	0.10	0.07	±0.05	(8.74, 8.65)
HD 36960	B0.5 V	28 900	3.9	5.9 ± 0.8	**8.71**	0.10	0.04	±0.03	(8.74, 8.68)
HD 37042	B0.7 V	29 700	4.2	4.9 ± 1.1	**8.75**	0.08	0.06	±0.02	(8.78, 8.74)
HD 36591	B1 V	27 200	4.1	4.5 ± 0.3	**8.71**	0.10	0.02	∓0.02	(8.71, 8.74)
HD 36959	B1 V	25 800	4.2	2.1 ± 0.4	**8.70**	0.06	0.02	∓0.05	(8.66, 8.76)
HD 37744	B1.5 V	23 800	4.1	3.6 ± 1.4	**8.70**	0.07	0.06	∓0.09	(8.61, 8.79)
HD 35299	B1.5 V	23 700	4.2	2.8 ± 0.6	**8.72**	0.07	0.03	∓0.09	(8.64, 8.82)
HD 36285	B2 V	20 600	4.0	5.5 ± 1.5	**8.80**	0.10	0.06	∓0.13	(8.67, 8.92)
HD 35039	B2 V	19 800	3.7	5.3 ± 1.5	**8.79**	0.07	0.07	∓0.15	(8.65, 8.94)
HD 36629	B2 V	20 000	4.1	6.0 ± 1.7	**8.76**	0.10	0.06	∓0.14	(8.62, 8.89)
HD 36430	B2 V	18 600	4.1	6.3 ± 2.2	**8.76**	0.07	0.08	∓0.13	(8.64, 8.90)
HD 35912	B2 V	18 500	4.0	6.3±2.2	**8.79**	0.09	0.08	∓0.13	(8.67, 8.93)

effective temperatures (but within the errors) and gravities ∼0.1–0.2 dex larger. Several factors produced this difference in the derived stellar parameters. First, we based our $T_{\rm eff}-\log g$ determination on the HSi analysis, instead of using the H and He I-II lines. The best $T_{\rm eff}$ - $\log g$ pair reproducing the Si III-IV ionization equilibrium and the wings of the H lines simultaneously is the one indicated in Table 3. A lower $\log g$ requested an effective temperature somewhat lower (which was not fitting the He II lines). In addition, the better quality of the new spectra allowed us to better constrain the gravity of the stars. The wings of the H lines are not very sensitive to changes of ∼0.1–0.2 dex in $\log g$ in this range of stellar parameters. In Simón-Díaz et al., we based our decision about the best solution on the faint He II λ4541 line; however, it is better to rely on the HSi criterion, which is more sensitive in this range of stellar parameters. In fact, we find that the new $T_{\rm eff}-\log g$ pair also fits nicely the He I-II lines. We thus prefer this last solution.

We also obtain ∼0.05–0.10 dex higher oxygen abundances. Part of this difference is caused by the change in stellar parameters; in addition, we measured sligthly larger *EW*s for the O II lines in both stars. Note, however, that the old and new abundances agree when taking the error bars into account. The discrepancy for these two objects between Simón-Díaz et al. (2006) and these new studies serves as an example of the effect of intrinsic uncertainties in determination of stellar abundances. Following a similar methodology the same author can find slightly different results (but within the errors) when analyzing spectra from two different observing campaigns[10].

Recently, Przybilla et al. (2008) analyzed a representative sample of unevolved early B-type stars in nearby OB associations and the field using a similar technique but a different stellar atmosphere code (line blanketed ATLAS9 LTE model atmospheres, Kurucz 1993) and NLTE line-formation calculations (with updated versions of DETAIL and SURFACE, Giddings 1981; Butler & Giddings 1985). They have one star in common with our work, HD 36591 (HR 1861). We obtain very similar results for the stellar parameters, as well as the Si and O abundances. They used several $T_{\rm eff}$ spectroscopic indicators (apart from Si II-IV), finding very good overall agreement.

Gummersbach et al. (1998) included a sample of 5 stars from Ori OB1 in their study of the abundance gradient of the Galaxy. We have three stars in common. Gummersbach et al. used a self-consistent spectroscopic approach. We find similar effective temperatures for the two hotter objects (when Si IV lines are available), but ∼0.2 dex lower gravities. For these stars (HD 36959 and HD 36960), the derived Si and O abundances agree (within the errors) with our values. The difference in gravity could explain their slightly lower O abundances.

Interestingly, for the cooler object in common (HD 35039), we obtained lower $T_{\rm eff}$ and $\log g$. It is remarkable that they obtained very low O and Si abundances (8.20 and 7.08 dex, respectively) for this star. Probably, this result is related to the Si II problem we described in Sect. 3.4 (see also lower panel in Fig. 2); they used line Si II 4130 to establish $T_{\rm eff}$, so obtained too high a value (23 500 K vs. 19 900 K, the value we obtained). For this range of stellar parameters, higher $T_{\rm eff}$ supposes lower O abundances, and a change of ∼3000 K in $T_{\rm eff}$ can perfectly explain a 0.5 dex variation in the O abundance.

Figure 5 presents a comparison our results with those obtained by Cunha & Lambert (1992, 1994) concerning the stellar parameters, Si and O abundances. There is a clear discrepancy for the majority of the objects, in terms not only of effective temperatures, but also of gravities. Cunha & Lambert (1992, 1994) made use of the calibrations of Strömgen photometry coupled with the fits to the pressure-broadened line wings of Hγ (from Kurucz 1979, LTE stellar atmopsheres) to derive $T_{\rm eff}$ and $\log g$. Following Gies & Lambert (1992), they adjusted the $T_{\rm eff}$ calibrations by Lester et al. (1986) and Balona (1984) upward by 4.2% and 5.2% , respectively. The discrepancy in effective temperatures obtained through commonly used photometric calibrations and spectroscopic line diagnostic has already been pointed out by several authors (e.g. Kilian et al. 1991; Nieva & Przybilla 2008). Our result once more brings out these discrepancies.

Note also the large discrepancy found for the gravity. The Cunha & Lambert values are systematically higher (∼0.3 dex). As shown by Nieva & Przybilla (2007), the use of LTE profiles for the gravity determination lead to overestimated $\log g$ values, in particular for hotter stars. In Fig. 3 we show a comparison of synthetic hydrogen lines from two FASTWIND models with the observed profiles for HD 36960 (labeled with #3 in Fig. 5. One of the models considers the stellar parameters derived from our analysis, the other one corresponds to the $T_{\rm eff}$-$\log g$ pair provided by Cunha & Lambert (1992). The difference in the wings of the lines is clear.

We also find big discrepancies in the derived Si and O abundance for most of the stars, with no systematic trend (i.e. differences are found in both positive and negative directions). There are several factors to take into account to explain this disagreement. One of them is the imprecise determination of

[10] The different results may also be caused by actual changes in the stellar spectra (e.g. due to binarity).

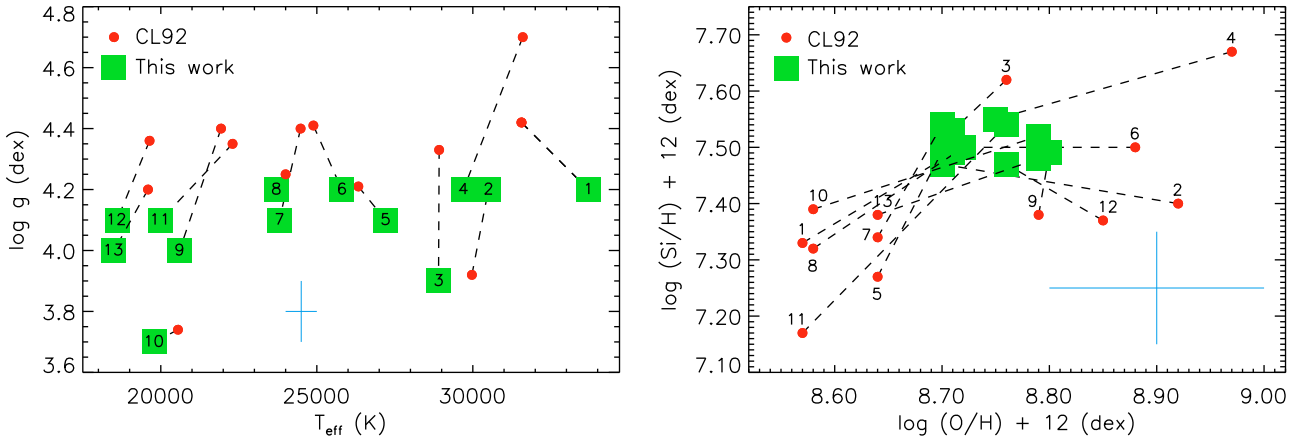

Fig. 5. Comparison of our derived stellar parameters, Si and O abundances, with those obtained by Cunha & Lambert (1992, 1994). Results from both studies for each star are connected by a dashed line. Numbers follow the order of stars presented in Tables 3 and 4. The size of the uncertainties of the various quantities are shown by the crosses.

the stellar parameters from photometric indices. But maybe the most important one is the following. Once the stellar parameters were calculated as described above, Cunha & Lambert use those values to perform the abundance analysis, computing line-blanketed LTE model atmospheres with ATLAS6 (Kurucz 1979) for the LTE case, or using a grid of *EW*s based on Gold's models (Gold 1984) for the NLTE abundance calculations. The risk in this strategy is that the stellar abundance analysis is decoupled of the stellar parameter determination, and this could produce inconsistencies in the analysis process. Briefly, the calculation of *EW*s of those lines used for the abundance determination is based on the stellar atmosphere structure defined by a stellar atmosphere model computed for a given set of stellar parameters; on the other hand, the stellar parameters derived for a given star will depend on the characteristics of the stellar atmosphere model we have used[11]. Therefore, it may be dangerous to do an abundance analysis with a given stellar atmosphere code using the stellar parameters obtained from a different code or a photometric calibration. This argument is crucial in the case of stars with $T_{\rm eff} \geq 30\,000$ K, where photometric methods become completely unreliable discriminators of temperatures and gravities, because of the insensitivity of the Rayleigh-Jeans tail of the spectral energy distribution on temperature.

A self-consistent spectroscopic approach allows minimizing this problem. In this case, the stellar parameters are determined by fitting certain spectroscopic diagnostics, and then the same models are used for the abundance analysis. This way we are certain that the stellar atmosphere structure used for the computation of the abundance diagnostics is coherent with the derived stellar parameters for the studied star. To a first order, when the whole analysis is performed with stellar atmosphere codes with different characteristics, the derived abundances should be quite similar (although the derived stellar parameters could be somewhat different). This approach can be strengthened if multiple independent spectroscopic indicators are considered (i.e. Si III-IV, He I-II, C II-IV; see e.g. this study or Nieva & Przybilla 2008).

[11] As an example, we want to mention the consequences that including the line blanketing and wind blanketing effects in the stellar atmosphere models of O and early B-type stars had on the SpT – $T_{\rm eff}$ calibrations of these stars (see e.g. Martins et al. 2005; Repolust et al. 2004).

5. Chemical composition of B-type stars in the Ori OB1 association

Figures 6 and 7 again show the derived oxygen and silicon abundances in our sample of B-type stars in the Ori OB1 association, along with the results by Cunha & Lambert (1994). This time, the stars are ordered following the subgroups suggested by Blaauw (1964). As discussed in Cunha & Lambert (1994), they found that the stars in the youngest group (Id) and some of the stars in subgroup Ic were enriched in oxygen by about 40% relative to the stars belonging to the older subgroups. They interpreted this result as possible proof of enrichment of the new generation of stars in the association with the products from supernovae ejecta from the older subgroups. In addition, they found features of this enrichment in silicon (also expected from the triggered star formation scenario). In contrast, we did not find any systematic difference between the O and Si abundances in stars from the various associations. In fact, our results indicate that the B-type stars in the Ori OB1 association are chemically homogeneous (at least in terms of oxygen and silicon), having a dispersion in abundances (0.04 and 0.03 dex, respectively) smaller than the intrinsic uncertainties of the derived abundances (0.10 and 0.08 dex, respectively). The mean abundances are ϵ(O) = 8.73 dex and ϵ(Si) = 7.51 dex. These values agree with those obtained by Przybilla et al. (2008) for their sample of six stars in the solar neighborhood.

5.1. Comparison with the Sun

We also include in Fig. 6 the resulting solar oxygen abundances appearing in the literature in the past 4 years (during the so-called solar oxygen crisis[12] epoch, not yet finished). Various authors have published values for the solar oxygen abundance based on improved model atmospheres (either 1D and 3D), line formation codes, atomic and molecular data, and detailed treatment of blends. In the plot, we present results by Centeno & Socas-Navarro (2008), Meléndez & Asplund (2008), Ayres (2008), Caffau et al. (2008), Allende Prieto (2008), Socas-Navarro & Norton (2007), Ayres et al. (2006), Asplund et al. (2004), and Grevesse & Sauval (1998). This last value (marked with an internal black dot) was considered as the standard solar O abundance until a few years ago. The derived solar

[12] Ayres et al. (2006)

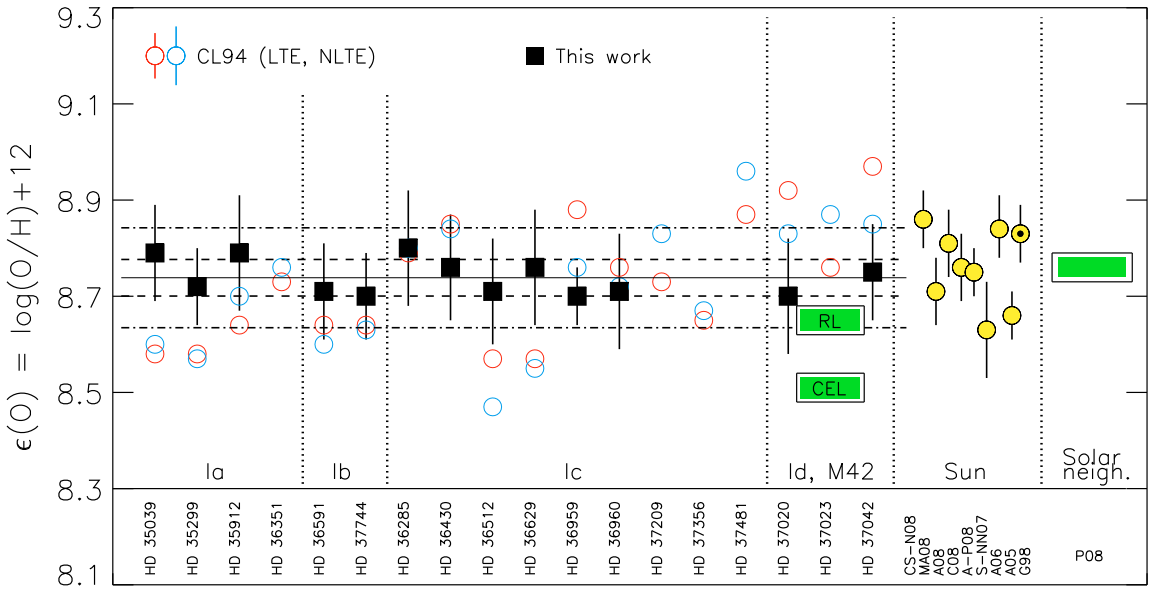

Fig. 6. Oxygen abundances derived for our sample of early B-type stars in the Orion association, and comparison with the previous results from Cunha & Lambert (1994). Vertical lines separates stars from the various subgroups. Solid and dashed horizontal lines represent the mean value and the dispersion (1σ) of our results; dot-dashed horizontal lines indicate the characteristic intrinsic uncertainty of the derived abundances (accounting for uncertainties in stellar parameters, microturbulence, and the line-by-line abundance dispersion). The oxygen abundance derived by Esteban et al. (2004) for M 42, along with the values determined for the Solar abundance in the past 4 years (the epoch of the "solar crisis"), are also presented for comparison.

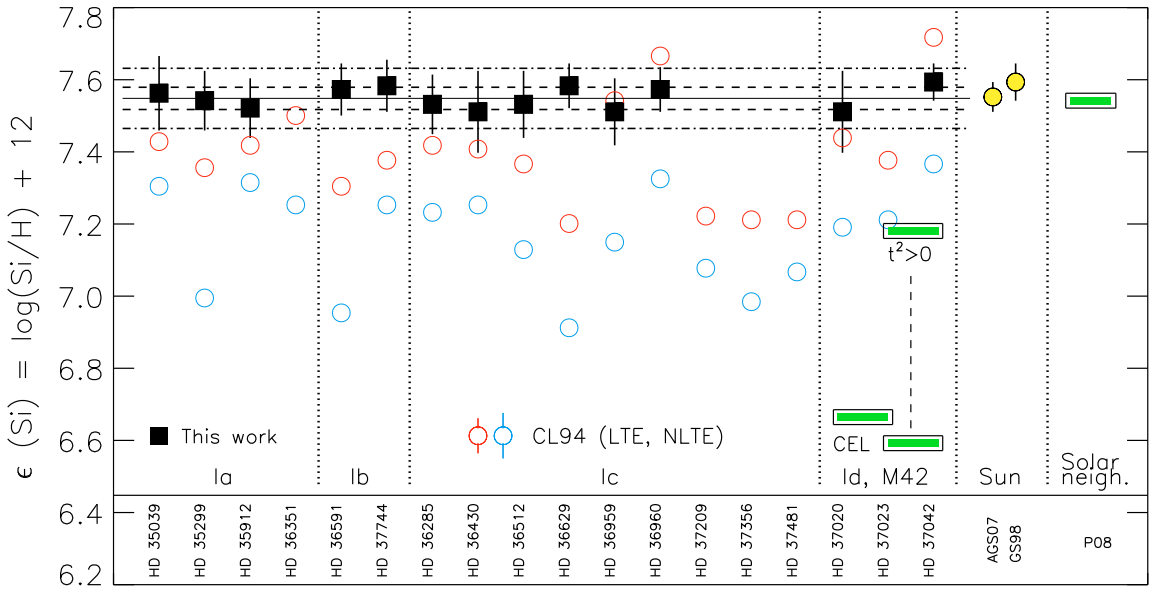

Fig. 7. As Fig. 2 but for silicon. This time, the reference for the nebular abundance is Rubin et al. (1993) and Garnett et al. (1995) (first and second column, see text). Solar values from Asplund et al. (2005) and Grevesse & Sauval (1998).

values range from 8.63 dex (Socas-Navarro & Norton 2007) to 8.86 dex (Centeno & Socas-Navarro 2008). The O abundances in our sample of stars in Ori OB1 lie in the middle of all these values. In view of the present-day results, the only thing we can say is that oxygen abundances in the Sun and B-type stars in the solar vicinity are the same within the uncertainties. However, we consider it too premature to draw any firm conclusion or hypothesis about the chemical evolution of the local interstellar medium during the lifetime of the Sun.

Figure 7 also shows a comparison of our derived Si abundances with the Solar value. We only present here the old abundance (Grevesse & Sauval 1998) and the new value proposed by Asplund et al. (2005). In contrast to previous results, the mean Si abundance in B-type stars in Ori OB1 is very close to the Solar value (similar to other B-type stars in the solar vicinity Przybilla et al. 2008).

5.2. Comparison with the Orion nebula

The most recent and detailed analysis of the optical spectrum of the Orion nebula was done by Esteban et al. (2004). The high-quality UVES@VLT spectrum they used allowed them to derive

the oxygen gas phase abundance of the nebula by using collisionally excited lines (CELs) and recombination lines (RLs). The final value they propose is 8.65 ± 0.03 dex. This value was calculated assuming the ionic abundances given by O^{2+} RLs and O^{+} CEL (plus a $t^2 = 0.022$)[13]. Note, however, the abundance given by the O^{2+} and O^{+} CELs (and t^2=0) is 8.51 ± 0.03 dex. These values have been included in Fig. 6 for comparison with the early B-type stellar abundances presented in this study. The mean value of the derived stellar oxygen abundances is 0.25 and 0.11 dex higher than the nebular abundances given by the CELs and RLs, respectively.

Although the mean stellar abundance seems to agree better with the one given by the faint recombination lines, we have to consider that the analysis of the nebular emission line spectrum can only provide abundances for the ionized gas phase of the ISM. This means a lower limit to the actual ISM abundance, since part of the oxygen can be depleted, forming part of the dust grains.

Silicon is one of the elements expected to be more depleted onto dust grains, along with Mg and Fe (Draine 2003). We can therefore compare our derived Si abundances with those obtained from the study of the emission line spectrum of the Orion nebula to try to find some clues about the amount of oxygen depleted. One should note that the determination of Si nebular abundances is not straightforward and must be based on results from photoionization models and certain ionization correction factors (ICFs). The only determinations of Si abundance in the Orion nebula we found in the literature are those by Rubin et al. (1993) and Garnett et al. (1995). Both studies used the same observations of the FUV Si III] $\lambda\lambda$1883, 1892, and C III] $\lambda\lambda$1907, 1909 lines to estimate the Si abundance, and obtained 6.65 and 6.58 dex, respectively. They computed photoionization models to obtain Si/H (Rubin et al. 1993) and the ICF needed to transform Si^{2+}/C^{2+} into Si/C, hence the C/O and O/H ratios to derive Si/H (Garnett et al. 1995). In addition, Garnett et al. (1995) discuss how the effect of assuming a $t^2 = 0.04$ (Peimbert et al. 1993) in the calculation of the C/O and O/H ratios could affect the derived Si abundance. They obtained log (Si/H)+12 = 7.14 dex for this case. These three values of the Si abundance are included in Fig. 7 for comparison with the stellar abundances. The difference between stellar and gas phase Si abundances are ∼1 dex, or ∼0.3 dex, depending on the nebular abundances we trust more.

Since a detailed comparison of stellar and nebular abundances in Ori OB1 and the Orion nebula within a dust-depletion scenario requires more extended study, which is beyond the scope of this paper, we decide to present a more detailed discussion in a separate paper (in preparation).

6. Summary and conclusion

In this work, we applied a self-consistent spectroscopic approach to determining of the stellar parameters, the Si and O abundances of a sample of early-B type stars from the various subgroups of the Ori OB1 association. We made use of a high-quality spectroscopic data set, obtained with FIES@NOT, and the modern NLTE, line-blanketed, spherically extended stellar atmosphere code FASTWIND.

We developed several IDL programs to automatically identify and measure the *EW* of metal lines in high-resolution spectra. We also constructed a grid of FASTWIND HHeSiO models optimized for the analysis of early B-type, main sequence stars.

The availability of a large number of Si II-III-IV lines in the FIES@NOT spectra allowed us to obtain the stellar parameters with high accuracy and detect some problems related to some Si lines commonly used for the stellar parameter and Si abundance determination. Once these problems were accounted for, a high degree of homogeneity was found for Si abundances in the analyzed sample of stars.

The oxygen abundance analysis also result in a small dispersion of abundances, in contrast to previous determinations. The mean oxygen and silicon abundances agree with those resulting from a similar analysis of a representative sample of unevolved early B-type stars in the solar vicinity (Przybilla et al. 2008). Both results indicate that abundances derived from these stellar objects are more homogeneous and metal-rich than previously though.

We also compared the O and Si stellar abundance in Ori OB1 with those obtained for the Sun during the epoch of the "solar crisis". The O abundances in our sample of stars in Ori OB1 lie in the middle of all these values. In view of the present-day results, the only thing we can say is that oxygen abundances in the Sun and B-type stars in the solar vicinity are the same within the uncertainties. However, we consider it too premature to draw any firm conclusion or hypothesis about the chemical evolution of the local interstellar medium during the lifetime of the Sun. Silicon abundances are also very similar (contrary to what was previously found from the study of B-type stars).

Finally, we compared the stellar abundances with those derived from the study of the emission line spectrum of the Orion nebula. In a forthcoming paper we will present a more detailed discussion accounting for the possible depletion of O, Si, Mg, and Fe into dust.

This work points out one more time the importance of self-consistent spectroscopic abundance analyses for determining of the chemical composition of the photospheres of OB-type stars. Photometric $T_{\rm eff}$ diagnostics must be treated with caution in the context of abundance analyses of these type of objects. It is also dangerous to combine the stellar parameters determined with any given code and the abundance analysis performed with a different code. Systematic errors inherent in those techniques, or possible biases between the various codes, can lead to incorrect abundances.

Acknowledgements. Financial support by the Spanish Ministerio de Ciencia e Innovación under the project AYA2008-06166-C03-01. This work has also been partially funded by the Spanish MICINN under the Consolider-Ingenio 2010 Program grant CSD2006-00070: First Science with the GTC (http://www.iac.es/consolider-ingenio-gtc). I am very grateful to A. Herrero (Spain), G. Stasinska (France), and D. Schaerer (Switzerland) for their support and hospitality during the development of this work. I also acknowledge A. Herrero, M. Urbaneja, D. Lennon, F. Najarro, C. Trundle, and N. Castro for fruitful discussions. J. Puls, N. Przybilla, F. Nieva, and M. Urbaneja for the careful reading of the first version of this paper and all their comments. Finally, I thank J. Puls for allowing me to use the stellar atmosphere code FASTWIND.

References

Allende Prieto, C. 2008, 14th Cambridge Workshop on Cool Stars, Stellar Systems, and the Sun, 384, 39
Asplund, M., Grevesse, N., Sauval, A. J., Allende Prieto, C., & Kiselman, D. 2004, A&A, 417, 751
Asplund, M., Grevesse, N., & Sauval, A. J. 2005, ASPC, 336, 25
Ayres, T. R. 2008, ApJ, 686, 731
Ayres, T. R., Plymate, C., & Keller, C. U. 2006, ApJS, 165, 618
Balona, L. A. 1984, MNRAS, 211, 973

[13] The t^2 parameter was introduced by Peimbert (1967) to account for temperature fluctuations in ionized nebulae. The temperature fluctuation scenario has been proposed to explain the CELs vs. RL abundance discrepancy (see García-Rojas & Esteban 2007, and references therein).

Becker, S. R., & Butler, K. 1988, A&A, 201, 232
Becker, S. R., & Butler, K. 1990, A&A, 235, 326
Blaauw, A. 1964, ARA&A, 2, 213
Briceño, C., Calvet, N., Hernández, J., et al. 2005, AJ, 129, 907
Brown, A. G. A., de Geus, E. J., & de Zeeuw, P. T. 1994, A&A, 289, 101
Caffau, E., Ludwig, H.-G., Steffen, M., et al. 2008, A&A, 488, 1031
Cantiello, M., Langer, N., Brott, I. et al. 2009, A&A, 499, 279
Cartledge, S. I. B., Lauroesch, J. T., Meyer, D. M., et al. 2006, ApJ, 641, 327
Carigi, L., Peimbert, M., Esteban, C., et al. 2005, ApJ, 623, 213
Centeno, R., & Socas-Navarro, H. 2008, ApJ, 682, L61
Chiappini, C., Romano, D., Matteucci, F. 2003, MNRAS, 339, 63
Cowie, L. L., Songaila, A., & York, D. G. 1979, ApJ, 230, 469
Crowther, P. A., Lennon, D. J., & Walborn, N. R. 2006, A&A, 446, 279
Cunha, K., & Lambert, D. L. 1992, ApJ, 399, 586
Cunha, K., & Lambert, D. L. 1994, ApJ, 426, 170
Draine, B. T. 2003, ARA&A, 41, 241
Esteban, C., Peimbert, M., García-Rojas, J., et al. 2004, MNRAS, 355, 229
García-Rojas, J., & Esteban, C. 2007, ApJ, 670, 457
Garnett, D. R., Dufour, R. J., Peimbert, M., et al. 1995, ApJ, 449, L77
Gies, D. R., & Lambert, D. L. 1992, ApJ, 387, 673
Gray, D. F. 1976, The Observation and analysis of Stellar Photospheres, 1st edn (Cambridge University Press)
Gold, M. 1984, Diplomarbeit, Ludwig-Maximilians-Universität München
Grevesse, N., & Sauval, A. J. 1998, Space Sci. Rev., 85, 161
Gummersbach, C. A., Kaufer, A., Schaefer, D. R., et al. 1998, A&A, 338, 881
Herrero, A., & Lennon, D. J. 2004, IAUS, 215, 209
Herrero, A., Kudritzki, R. P., Vilchez, J. M., et al. 1992, A&A, 261, 209
Kilian, J. 1992, A&A, 262, 171
Kilian, J., Becker, S. R., Gehren, T., et al. 1991, A&A, 244, 419
Kurucz, R. L. 1979, ApJS, 40, 1
Lester, J. B., Gray, R. O., & Kurucz, R. L. 1986, ApJS, 61, 509
Martins, F., Schaerer, D., & Hillier, D. J. 2005, A&A, 436, 1049
Markova, N., & Puls, J. 2008, A&A, 478, 823
Meyer, D. M., Jura, M., & Cardelli, J. A. 1998, ApJ, 493, 222
Meléndez, J., & Asplund, M. 2008, A&A, 490, 817
Morel, T. 2009, CoAst, 158, 122
Nieva, M.-F., & Przybilla, N. 2007, A&A, 467, 295
Nieva, M.-F., & Przybilla, N. 2008, A&A, 481, 199
Nieva M.-F., & Przybilla, N. 2009, in Hot And Cool: Bridging Gaps in Massive Star Evolution, ed. C. Leitherer et al., ASP Conf. Ser. in press [arXiv:0902.2949]
Peimbert, M. 1967, ApJ, 150, 825
Peimbert, M., Storey, P. J., & Torres-Peimbert, S. 1993, ApJ, 414, 626
Przybilla, N., Nieva, M.-F., & Butler, K. 2008, ApJ, 688, L103
Puls, J., Urbaneja, M. A., Venero, R., et al. 2005, A&A, 435, 669
Repolust, T., Puls, J., Herrero, A. 2004, A&A, 415, 349
Reynolds, R. J., & Ogden, P. M. 1979, ApJ, 229, 942
Rubin, R. H., Dufour, R. J., & Walter, D. K. 1993, ApJ, 413, 242
Santolaya-Rey, A. E., Puls, J., & Herrero, A. 1997, A&A, 323, 488
Simón-Díaz, S. 2005, Thesis, Univ. de La Laguna, Spain
Simón-Díaz, S., & Herrero, A. 2007, A&A, 468, 1063
Simón-Díaz, S., Herrero, A., Esteban, C., et al. 2006, A&A, 448, 351
Socas-Navarro, H., & Norton, A. A. 2007, ApJ, 660, L153
Trundle, C., Lennon, D. J., Puls, J., et al. 2004, A&A, 417, 217
Urbaneja, M. A., Herrero, A., Kudritzki, R.-P., et al. 2005, ApJ, 635, 311

Pages 13 to 21 are available in the electronic edition of the journal at http://www.aanda.org

Table 5. List of $\log gf$ values for the Si II-IV lines considered in this study (from Atomic Line List v2.05). For the O II lines we refer to Simón-Díaz et al. (2006).

Ion	λ Å	$\log gf$	Configuration	Term
Si II	3856.02	–0.4569	3s $3p^2$-$3s^2$ (1S) 4p	2D-2Po
Si II	3862.60	–0.7130	3s $3p^2$-$3s^2$ (1S) 4p	2D-2Po
Si II	4128.10	0.3646	$3s^2$ (1S) 3d-$3s^2$ (1S) 4f	2D-2Fo
Si II	4130.90	0.5192	$3s^2$ (1S) 3d-$3s^2$ (1S) 4f	2D-2Fo
Si II	5041.02	0.2543	$3s^2$ (1S) 4p-$3s^2$ (1S) 4d	2Po-2D
Si II	5055.98	0.5083	$3s^2$ (1S) 4p-$3s^2$ (1S) 4d	2Po-2D
Si II	5056.32	–0.4460	$3s^2$ (1S) 4p-$3s^2$ (1S) 4d	2Po-2D
Si II	6347.11	0.1819	$3s^2$ (1S) 4s-$3s^2$ (1S) 4p	2S-2Po
Si II	6371.37	–0.1208	$3s^2$ (1S) 4s-$3s^2$ (1S) 4p	2S-2Po
Si III	4552.62	0.2828	3s 4s-3s 4p	3S-3Po
Si III	4567.84	0.0595	3s 4s-3s 4p	3S-3Po
Si III	4574.76	–0.4183	3s 4s-3s 4p	3S-3Po
Si III	5739.73	–0.1032	3s 4s-3s 4p	1S-1Po
Si IV	4088.86	0.1984	$2p^6$ 4s-$2p^6$ 4p	2S-2Po
Si IV	4116.10	–0.1055	$2p^6$ 4s-$2p^6$ 4p	2S-2Po
Si IV	4212.40	0.3840	$2p^6$ 5d-$2p^6$ 6f	2D-2Fo
Si IV	4212.41	0.5601	$2p^6$ 5d-$2p^6$ 6f	2D-2Fo
Si IV	4631.24	1.2158	$2p^6$ 5f-$2p^6$ 6g	2Fo-2G

Table 6. Results from the abundance analysis of HD 36512 (B0 V).

HD 36512	$T_{\rm eff}$ = 33 700 K, $\log g$ = 4.2 dex			$\xi_{\rm t}$(Si)=4.3
Line	EW (mÅ)	ΔEW (mÅ)	$\epsilon_{\rm Si}$ (dex)	$\Delta\epsilon_{\rm Si}$ (dex)
SiIII4552	117	4	7.51	0.07
SiIII4567	99	5	7.58	0.08
SiIII4574	50	4	7.53	0.09
SiIV4089	189	5	7.42	0.06
SiIV4116	166	5	7.54	0.07
SiIV4212	53	3	7.46	0.06
SiIV4631	75	4	7.40	0.06
			$\epsilon_{\rm Si}$ = **7.49**	$\Delta\epsilon_{\rm Si}(\sigma)$ = 0.07
	$\Delta\xi_{\rm t}$(Si) = 0.7		⇒	$\Delta\epsilon_{\rm Si}(\xi_{\rm t})$ = 0.05

HD 36512	$T_{\rm eff}$ = 33 700 K, $\log g$ = 4.2 dex			$\xi_{\rm t}$(O)=4.4
Line	EW (mÅ)	ΔEW (mÅ)	$\epsilon_{\rm O}$ (dex)	$\Delta\epsilon_{\rm O}$ (dex)
OII3945	36	5	8.81	0.13
OII3954	63	5	8.86	0.09
OII3982	29	5	8.63	0.14
OII4317	78	11	8.74	0.16
OII4319	75	5	8.77	0.08
OII4366	70	8	8.70	0.14
OII4414	89	6	8.55	0.09
OII4416	76	9	8.66	0.15
OII4452	25	10	8.59	0.33
OII4641	95	12	8.69	0.20
OII4661	82	4	8.88	0.07
OII4673	23	3	8.83	0.12
OII4676	61	5	8.67	0.10
OII4696	13	6	8.73	0.37
OII6721	30	8	8.71	0.20
OII4072	84	8	8.62	0.15
OII4076	101	6	8.64	0.11
OII4078	33	6	8.73	0.18
OII4086	48	8	8.88	0.20
OII4089	77	6	8.63	0.10
OII4891	19	5	8.65	0.20
OII4906	34	5	8.67	0.13
OII4943	46	3	8.59	0.06
			$\epsilon_{\rm O}$ = **8.71**	$\Delta\epsilon_{\rm O}(\sigma)$ = 0.10
	$\Delta\xi_{\rm t}$(O) = 1.5		⇒	$\Delta\epsilon_{\rm O}(\xi_{\rm t})$ = 0.05

Table 7. Results from the abundance analysis of HD 37020 (B0.5 V).

HD 37020	$T_{\rm eff}$ = 30 500 K, $\log g$ = 4.2 dex			$\xi_{\rm t}$(Si) = 0.5
Line	EW (mÅ)	ΔEW (mÅ)	$\epsilon_{\rm Si}$ (dex)	$\Delta\epsilon_{\rm Si}$ (dex)
SiIII4552	130	13	7.56	0.27
SiIII4567	110	7	7.54	0.14
SiIII4574	74	9	7.57	0.22
SiIII5739	73	9	7.38	0.19
SiIV4089	104	21	7.29	0.42
SiIV4116	90	8	7.41	0.17
SiIV4212	25	5	7.43	0.21
SiIV4631	47	7	7.55	0.17
			$\epsilon_{\rm Si}$ = **7.47**	$\Delta\epsilon_{\rm Si}(\sigma)$ = 0.10
	$\Delta\xi_{\rm t}$(Si) = 0.5		⇒	$\Delta\epsilon_{\rm Si}(\xi_{\rm t})$ = 0.04

HD 37020	$T_{\rm eff}$ = 30500 K, $\log g$ = 4.2 dex			$\xi_{\rm t}$(O)=6.4
OII3945	56	10	8.75	0.19
OII3954	90	10	8.77	0.15
OII4317	94	10	8.56	0.13
OII4319	106	13	8.73	0.18
OII4366	104	13	8.71	0.19
OII4414	130	10	8.50	0.12
OII4416	119	10	8.68	0.13
OII4452	62	12	8.83	0.21
OII4638	101	10	8.83	0.15
OII4641	141	10	8.73	0.14
OII4661	105	10	8.71	0.15
OII4676	94	12	8.67	0.19
OII6721	61	12	8.77	0.19
OII4076	144	10	8.73	0.15
OII4891	40	8	8.84	0.19
OII4906	48	9	8.63	0.18
OII4941	48	6	8.57	0.12
OII4943	65	8	8.53	0.13
			$\epsilon_{\rm O}$ = **8.70**	$\Delta\epsilon_{\rm O}(\sigma)$ = 0.10
	$\Delta\xi_{\rm t}$(O) = 1.6		⇒	$\Delta\epsilon_{\rm O}(\xi_{\rm t})$ = 0.07

Table 8. Results from the abundance analysis of HD 36960 (B0.5 V).

HD 36960	$T_{\rm eff}$ = 28 900 K, log g = 3.9 dex			$\xi_{\rm t}$(Si)=5.4
Line	EW (mÅ)	ΔEW (mÅ)	$\epsilon_{\rm Si}$ (dex)	$\Delta\epsilon_{\rm Si}$ (dex)
SiIII4552	211	5	7.53	0.06
SiIII4567	179	5	7.51	0.06
SiIII4574	116	5	7.52	0.07
SiIV4089	160	11	7.55	0.15
SiIV4116	127	9	7.52	0.14
SiIV4212	28	4	7.50	0.14
SiIV4631	37	3	7.54	0.08
			$\epsilon_{\rm Si}$ **= 7.53**	$\Delta\epsilon_{\rm Si}(\sigma) = 0.02$
	$\Delta\xi_{\rm t}$(Si) = 0.6		$\Rightarrow$	$\Delta\epsilon_{\rm Si}(\xi_{\rm t}) = 0.06$
HD 36960	$T_{\rm eff}$ = 28 900 K, log g = 3.9 dex			$\xi_{\rm t}$(O)=5.9
OII3945	68	6	8.78	0.11
OII3954	96	7	8.71	0.10
OII3982	61	6	8.63	0.11
OII4317	125	7	8.71	0.08
OII4319	125	6	8.78	0.08
OII4366	113	5	8.66	0.07
OII4414	165	5	8.66	0.06
OII4416	141	5	8.75	0.06
OII4452	50	5	8.54	0.10
OII4661	127	5	8.87	0.08
OII4673	46	5	8.85	0.12
OII4676	101	5	8.66	0.08
OII4696	30	3	8.78	0.09
OII6641	47	6	8.81	0.12
OII6721	76	9	8.77	0.12
OII4078	60	4	8.81	0.09
OII4891	34	10	8.64	0.27
OII4906	61	6	8.71	0.11
OII4941	54	10	8.54	0.19
OII4943	75	4	8.54	0.06
OII4956	23	4	8.72	0.14
			$\epsilon_{\rm O}$ **= 8.71**	$\Delta\epsilon_{\rm O}(\sigma) = 0.10$
	$\Delta\xi_{\rm t}$(O) = 0.8		$\Rightarrow$	$\Delta\epsilon_{\rm O}(\xi_{\rm t}) = 0.04$

Table 9. Results from the abundance analysis of HD 37042 (B0.7 V).

HD 37042	$T_{\rm eff}$ = 29 700 K, log g = 4.2 dex			$\xi_{\rm t}$(Si)=1.4
Line	EW (mÅ)	ΔEW (mÅ)	$\epsilon_{\rm Si}$ (dex)	$\Delta\epsilon_{\rm Si}$ (dex)
SiIII4552	149	2	7.54	0.04
SiIII4567	133	6	7.59	0.11
SiIII4574	88	4	7.56	0.08
SiIII5739	99	7	7.50	0.13
SiIV4116	95	10	7.53	0.21
SiIV4212	24	5	7.54	0.22
SiIV4631	35	10	7.55	0.30
			$\epsilon_{\rm Si}$ **= 7.55**	$\Delta\epsilon_{\rm Si}(\sigma) = 0.03$
	$\Delta\xi_{\rm t}$(Si) = 0.3		$\Rightarrow$	$\Delta\epsilon_{\rm Si}(\xi_{\rm t}) = 0.04$
HD 37042	$T_{\rm eff}$ = 29 700 K, log g = 4.2 dex			$\xi_{\rm t}$(O)=4.9
OII3945	68	6	8.87	0.11
OII3954	93	7	8.79	0.12
OII4317	116	10	8.75	0.13
OII4319	116	11	8.84	0.16
OII4366	108	9	8.76	0.14
OII4414	143	10	8.64	0.13
OII4416	127	7	8.78	0.10
OII4452	64	6	8.82	0.12
OII4641	142	7	8.81	0.11
OII4661	108	5	8.79	0.09
OII4676	95	6	8.71	0.11
OII4696	30	5	8.82	0.16
OII4072	110	10	8.62	0.18
OII4076	128	10	8.63	0.17
OII4078	57	8	8.84	0.19
OII4891	39	5	8.80	0.13
OII4906	57	5	8.75	0.10
OII4941	53	4	8.63	0.08
OII4943	73	4	8.63	0.07
OII4956	23	8	8.79	0.29
			$\epsilon_{\rm O}$ **= 8.75**	$\Delta\epsilon_{\rm O}(\sigma) = 0.08$
	$\Delta\xi_{\rm t}$(O) = 1.1		$\Rightarrow$	$\Delta\epsilon_{\rm O}(\xi_{\rm t}) = 0.06$

Table 10. Results from the abundance analysis of HD 36591 (B1 V).

HD 36591	$T_{\rm eff}$ = 27 200 K, log g = 4.1 dex			$\xi_{\rm t}$(Si)=1.3
Line	EW (mÅ)	ΔEW (mÅ)	$\epsilon_{\rm Si}$ (dex)	$\Delta\epsilon_{\rm Si}$ (dex)
SiIII4552	158	2	7.52	0.03
SiIII4567	145	2	7.62	0.04
SiIII4574	104	2	7.65	0.04
SiIII5739	114	2	7.56	0.03
SiIV4089	80	2	7.54	0.05
SiIV4116	61	2	7.48	0.06
			$\epsilon_{\rm Si}$ **= 7.53**	$\Delta\epsilon_{\rm Si}(\sigma) = 0.06$
	$\Delta\xi_{\rm t}$(Si) = 0.3		$\Rightarrow$	$\Delta\epsilon_{\rm Si}(\xi_{\rm t}) = 0.03$
HD 36591	$T_{\rm eff}$ = 27 200 K, log g = 4.1 dex			$\xi_{\rm t}$(O)=4.5
OII3945	69	2	8.80	0.04
OII3954	86	2	8.64	0.04
OII3982	62	2	8.64	0.04
OII4317	125	5	8.77	0.06
OII4319	114	2	8.76	0.03
OII4366	102	4	8.62	0.07
OII4414	144	2	8.61	0.03
OII4416	124	8	8.70	0.12
OII4452	53	3	8.59	0.07
OII4638	109	2	8.94	0.04
OII4641	145	2	8.84	0.03
OII4650	159	4	8.62	0.06
OII4661	113	2	8.83	0.03
OII4673	44	5	8.81	0.13
OII4676	97	4	8.70	0.07
OII4696	30	3	8.74	0.10
OII6641	48	2	8.90	0.04
OII6721	69	2	8.79	0.03
OII4072	113	7	8.65	0.13
OII4076	133	4	8.70	0.07
OII4078	56	3	8.77	0.08
OII4086	68	6	8.83	0.14
OII4891	34	3	8.67	0.09
OII4906	53	3	8.67	0.07
OII4941	48	2	8.54	0.04
OII4943	68	3	8.57	0.06
OII4956	24	3	8.77	0.11
			$\epsilon_{\rm O}$ **= 8.71**	$\Delta\epsilon_{\rm O}(\sigma) = 0.10$
	$\Delta\xi_{\rm t}$(O) = 0.3		$\Rightarrow$	$\Delta\epsilon_{\rm O}(\xi_{\rm t}) = 0.04$

Table 11. Results from the abundance analysis of HD 36959 (B1 V).

HD 36959	$T_{\rm eff}$ = 25 800 K, log g = 4.2 dex			$\xi_{\rm t}$(Si)=0.0
Line	EW (mÅ)	ΔEW (mÅ)	$\epsilon_{\rm Si}$ (dex)	$\Delta\epsilon_{\rm Si}$ (dex)
SiII4128	16	3	7.52	0.12
SiII4130	17	3	7.44	0.12
SiIII4552	142	1	7.48	0.02
SiIII4567	124	1	7.48	0.02
SiIII4574	90	1	7.54	0.02
SiIII5739	99	2	7.51	0.04
SiIV4089	45	1	7.45	0.04
SiIV4116	36	3	7.47	0.12
			$\epsilon_{\rm Si}$ **= 7.49**	$\Delta\epsilon_{\rm Si}(\sigma) = 0.03$
	$\Delta\xi_{\rm t}$(Si) = 0.5		$\Rightarrow$	$\Delta\epsilon_{\rm Si}(\xi_{\rm t}) = 0.07$
HD 36959	$T_{\rm eff}$ = 25 800 K, log g = 4.2 dex			$\xi_{\rm t}$(O)=2.1
OII3945	55	2	8.78	0.05
OII3954	73	2	8.69	0.04
OII3982	50	2	8.63	0.05
OII4317	98	6	8.76	0.10
OII4319	86	3	8.69	0.06
OII4366	81	5	8.62	0.10
OII4414	116	2	8.64	0.03
OII4416	99	3	8.72	0.05
OII4452	45	2	8.62	0.05
OII4641	113	2	8.75	0.04
OII4650	133	5	8.65	0.08
OII4661	89	2	8.76	0.04
OII4673	35	2	8.72	0.07
OII4676	75	3	8.61	0.07
OII4696	25	2	8.69	0.08
OII6641	30	2	8.78	0.06
OII6721	48	2	8.75	0.04
OII4072	94	6	8.72	0.13
OII4076	108	6	8.73	0.12
OII4078	46	3	8.80	0.09
OII4086	48	3	8.70	0.09
OII4891	26	2	8.67	0.07
OII4906	40	2	8.67	0.06
OII4941	39	2	8.62	0.06
OII4943	55	2	8.66	0.05
			$\epsilon_{\rm O}$ **= 8.70**	$\Delta\epsilon_{\rm O}(\sigma) = 0.02$
	$\Delta\xi_{\rm t}$(O) = 0.4		$\Rightarrow$	$\Delta\epsilon_{\rm O}(\xi_{\rm t}) = 0.06$

Table 12. Results from the abundance analysis of HD 37744 (B1.5 V).

HD 37744	$T_{\rm eff}$ = 23 800 K, log g = 4.1 dex			$\xi_{\rm t}$(Si)=0.5
Line	EW (mÅ)	ΔEW (mÅ)	$\epsilon_{\rm Si}$ (dex)	$\Delta\epsilon_{\rm Si}$ (dex)
SiII3856	20	4	7.49	0.22
SiII6371	18	6	7.57	0.22
SiIII4552	147	3	7.57	0.05
SiIII4567	120	4	7.49	0.07
SiIII4574	88	4	7.59	0.09
SiIII5739	86	4	7.45	0.08
SiIV4116	23	4	7.56	0.26
			$\epsilon_{\rm Si}$ **= 7.53**	$\Delta\epsilon_{\rm Si}(\sigma) = 0.05$
	$\Delta\xi_{\rm t}$(Si) = 0.5		$\Rightarrow$	$\Delta\epsilon_{\rm Si}(\xi_{\rm t}) = 0.04$
HD 37744	$T_{\rm eff}$ = 23 800 K, log g = 4.1 dex			$\xi_{\rm t}$(O)=3.6
OII3945	45	5	8.73	0.13
OII3954	66	7	8.72	0.15
OII4317	72	7	8.60	0.13
OII4319	73	8	8.67	0.16
OII4366	67	6	8.56	0.13
OII4414	100	14	8.62	0.23
OII4416	76	7	8.59	0.14
OII4452	32	6	8.51	0.20
OII4641	99	5	8.76	0.09
OII4650	123	8	8.71	0.13
OII4661	79	5	8.81	0.10
OII4673	25	5	8.67	0.20
OII4676	71	6	8.76	0.13
OII4696	20	5	8.73	0.23
OII6721	33	7	8.74	0.19
OII4069	136	13	8.83	0.18
OII4078	36	6	8.71	0.21
OII4906	32	4	8.69	0.13
OII4941	30	5	8.62	0.17
OII4943	45	5	8.69	0.13
OII4956	14	3	8.79	0.17
			$\epsilon_{\rm O}$ **= 8.70**	$\Delta\epsilon_{\rm O}(\sigma) = 0.07$
	$\Delta\xi_{\rm t}$(O) = 1.4		$\Rightarrow$	$\Delta\epsilon_{\rm O}(\xi_{\rm t}) = 0.06$

Table 13. Results from the abundance analysis of HD 35299 (B1.5 V).

HD 35299	$T_{\rm eff}$ = 23 700 K, log g = 4.2 dex			$\xi_{\rm t}$(Si)=0.5
Line	EW (mÅ)	ΔEW (mÅ)	$\epsilon_{\rm Si}$ (dex)	$\Delta\epsilon_{\rm Si}$ (dex)
SiII3856	27	5	7.65	0.24
SiII3862	15	2	7.44	0.13
SiII6371	23	4	7.64	0.13
SiIII4552	133	5	7.45	0.08
SiIII4567	110	2	7.40	0.04
SiIII4574	79	2	7.50	0.05
SiIII5739	81	2	7.47	0.04
SiIV4089	26	1	7.59	0.06
SiIV4116	18	2	7.48	0.15
			$\epsilon_{\rm Si}$ **= 7.50**	$\Delta\epsilon_{\rm Si}(\sigma) = 0.08$
	$\Delta\xi_{\rm t}$(Si) = 0.5		$\Rightarrow$	$\Delta\epsilon_{\rm Si}(\xi_{\rm t}) = 0.02$
HD 35299	$T_{\rm eff}$ = 23 700 K, log g = 4.2 dex			$\xi_{\rm t}$(O)=2.8
OII3945	44	2	8.81	0.06
OII3954	59	2	8.72	0.05
OII3982	38	2	8.62	0.06
OII4317	78	5	8.80	0.09
OII4319	66	3	8.69	0.07
OII4366	61	3	8.59	0.07
OII4414	95	5	8.70	0.09
OII4416	80	2	8.77	0.04
OII4452	32	2	8.61	0.07
OII4641	91	5	8.79	0.10
OII4650	112	5	8.73	0.09
OII4661	68	3	8.77	0.07
OII4673	25	2	8.76	0.08
OII4676	59	2	8.68	0.05
OII4696	17	2	8.70	0.10
OII6641	18	2	8.82	0.09
OII6721	29	3	8.77	0.09
OII4072	82	3	8.81	0.07
OII4076	94	4	8.79	0.08
OII4078	35	2	8.79	0.07
OII4086	36	2	8.67	0.07
OII4891	16	3	8.64	0.16
OII4906	28	2	8.70	0.07
OII4941	25	2	8.59	0.08
OII4943	40	2	8.71	0.06
OII4956	12	2	8.78	0.13
			$\epsilon_{\rm O}$ **= 8.72**	$\Delta\epsilon_{\rm O}(\sigma) = 0.07$
	$\Delta\xi_{\rm t}$(O) = 0.6		$\Rightarrow$	$\Delta\epsilon_{\rm O}(\xi_{\rm t}) = 0.03$

Table 14. Results from the abundance analysis of HD 36285 (B2 V).

HD 36285	$T_{\rm eff}$ = 20600 K, log g = 4.0 dex			$\xi_{\rm t}$(Si)=1.7
Line	EW (mÅ)	ΔEW (mÅ)	$\epsilon_{\rm Si}$ (dex)	$\Delta\epsilon_{\rm Si}$ (dex)
SiII3856	41	2	7.38	0.07
SiII3862	37	5	7.52	0.19
SiII6347	61	4	7.60	0.09
SiII6371	45	3	7.53	0.08
SiIII4552	110	1	7.49	0.02
SiIII4567	88	2	7.44	0.04
SiIII4574	59	1	7.51	0.03
SiIII5739	53	2	7.46	0.05
			$\epsilon_{\rm Si}$ **= 7.49**	$\Delta\epsilon_{\rm Si}(\sigma)$ = 0.06
	$\Delta\xi_{\rm t}$(Si) = 0.5		⇒	$\Delta\epsilon_{\rm Si}(\xi_{\rm t})$ = 0.05
HD 36285	$T_{\rm eff}$ = 20 600 K, log g = 4.0 dex			$\xi_{\rm t}$(O)=5.5
OII3945	26	3	8.79	0.12
OII3954	41	3	8.79	0.09
OII4317	46	5	8.74	0.12
OII4319	42	3	8.69	0.08
OII4366	42	4	8.65	0.11
OII4414	63	3	8.70	0.06
OII4416	50	3	8.74	0.07
OII4452	26	3	8.88	0.12
OII4638	46	3	8.94	0.08
OII4650	78	4	8.70	0.07
OII4661	46	2	8.80	0.05
OII4673	12	3	8.68	0.21
OII4676	36	3	8.66	0.09
OII6721	15	4	8.99	0.23
OII4069	81	6	8.86	0.10
OII4072	55	4	8.80	0.11
OII4078	24	4	8.91	0.19
OII4086	24	10	8.78	0.48
OII4906	16	3	8.85	0.17
OII4941	16	5	8.84	0.29
OII4943	25	3	8.91	0.12
			$\epsilon_{\rm O}$ **= 8.80**	$\Delta\epsilon_{\rm O}(\sigma)$ = 0.10
	$\Delta\xi_{\rm t}$(O) = 1.5		⇒	$\Delta\epsilon_{\rm O}(\xi_{\rm t})$ = 0.06

Table 15. Results from the abundance analysis of HD 35039 (B2 V).

HD 35039	$T_{\rm eff}$ = 19 800 K, log g = 3.7 dex			$\xi_{\rm t}$(Si)=3.3
Line	EW (mÅ)	ΔEW (mÅ)	$\epsilon_{\rm Si}$ (dex)	$\Delta\epsilon_{\rm Si}$ (dex)
SiII3856	61	2	7.63	0.06
SiII3862	45	5	7.54	0.15
SiII6347	75	10	7.51	0.17
SiII6371	55	2	7.46	0.04
SiIII4552	125	10	7.49	0.15
SiIII4567	103	5	7.47	0.09
SiIII4574	67	5	7.52	0.11
SiIII5739	69	5	7.58	0.10
			$\epsilon_{\rm Si}$ **= 7.52**	$\Delta\epsilon_{\rm Si}(\sigma)$ = 0.06
	$\Delta\xi_{\rm t}$(Si) = 1.0		⇒	$\Delta\epsilon_{\rm Si}(\xi_{\rm t})$ = 0.08
HD 35039	$T_{\rm eff}$ = 19 800 K, log g = 3.7 dex			$\xi_{\rm t}$(O)=5.3
OII3945	31	2	8.91	0.07
OII3954	41	2	8.79	0.06
OII3982	25	2	8.69	0.08
OII4317	50	6	8.80	0.14
OII4319	45	4	8.74	0.11
OII4414	64	2	8.72	0.04
OII4416	54	4	8.82	0.10
OII4641	64	3	8.80	0.07
OII4650	82	2	8.74	0.04
OII4661	46	3	8.79	0.08
OII4673	15	4	8.79	0.25
OII4676	39	2	8.71	0.06
OII4069	80	3	8.88	0.05
OII4072	59	3	8.91	0.08
OII4078	21	4	8.84	0.21
OII4086	25	4	8.84	0.18
OII4941	12	3	8.68	0.21
OII4943	21	3	8.81	0.14
			$\epsilon_{\rm O}$ **= 8.79**	$\Delta\epsilon_{\rm O}(\sigma)$ = 0.07
	$\Delta\xi_{\rm t}$(O) = 1.5		⇒	$\Delta\epsilon_{\rm O}(\xi_{\rm t})$ = 0.07

Table 16. Results from the abundance analysis of HD 36629 (B2 V).

HD 36629	$T_{\rm eff}$ = 20 000 K, log g = 4.1 dex			$\xi_{\rm t}$(Si)=1.0
Line	EW (mÅ)	ΔEW (mÅ)	$\epsilon_{\rm Si}$ (dex)	$\Delta\epsilon_{\rm Si}$ (dex)
SiII3856	52	2	7.58	0.07
SiII3862	42	2	7.55	0.08
SiII6347	65	3	7.62	0.07
SiII6371	48	2	7.53	0.06
SiIII4552	90	1	7.52	0.02
SiIII4567	73	1	7.49	0.02
SiIII4574	46	1	7.51	0.03
SiIII5739	42	2	7.53	0.06
			$\epsilon_{\rm Si}$ = **7.54**	$\Delta\epsilon_{\rm Si}(\sigma)$ = 0.04
	$\Delta\xi_{\rm t}$(Si) = 0.5		⇒	$\Delta\epsilon_{\rm Si}(\xi_{\rm t})$ = 0.05
HD 36629	$T_{\rm eff}$ = 20 000 K, log g = 4.1 dex			$\xi_{\rm t}$(O)=6.0
OII3945	24	2	8.91	0.09
OII3954	28	2	8.68	0.07
OII4317	37	3	8.77	0.09
OII4319	30	2	8.63	0.07
OII4366	30	2	8.59	0.07
OII4414	50	2	8.69	0.05
OII4416	40	2	8.75	0.06
OII4452	16	1	8.74	0.06
OII4638	36	1	8.95	0.03
OII4641	41	1	8.63	0.03
OII4650	59	3	8.65	0.07
OII4661	32	2	8.72	0.07
OII4673	11	3	8.82	0.23
OII4676	27	2	8.65	0.07
OII4069	64	3	8.88	0.06
OII4072	45	2	8.83	0.06
OII4076	55	3	8.85	0.08
OII4078	15	2	8.79	0.13
OII4943	16	3	8.83	0.17
			$\epsilon_{\rm O}$ = **8.76**	$\Delta\epsilon_{\rm O}(\sigma)$ = 0.10
	$\Delta\xi_{\rm t}$(O) = 1.7		⇒	$\Delta\epsilon_{\rm O}(\xi_{\rm t})$ = 0.06

Table 17. Results from the abundance analysis of HD 36430 (B2 V).

HD 36430	$T_{\rm eff}$ = 18 400 K, log g = 4.1 dex			$\xi_{\rm t}$(Si)=3.5
Line	EW (mÅ)	ΔEW (mÅ)	$\epsilon_{\rm Si}$ (dex)	$\Delta\epsilon_{\rm Si}$ (dex)
SiII3862	61	5	7.43	0.13
SiII6347	100	10	7.57	0.16
SiII6371	74	6	7.49	0.12
SiIII4552	77	3	7.55	0.06
SiIII4567	53	2	7.40	0.05
SiIII4574	28	5	7.37	0.19
SiIII5739	25	2	7.47	0.08
			$\epsilon_{\rm Si}$ = **7.47**	$\Delta\epsilon_{\rm Si}(\sigma)$ = 0.08
	$\Delta\xi_{\rm t}$(Si) = 1.0		⇒	$\Delta\epsilon_{\rm Si}(\xi_{\rm t})$ = 0.07
HD 36430	$T_{\rm eff}$ = 18 400 K, log g = 4.1 dex			$\xi_{\rm t}$(O)=6.3
OII3954	19	5	8.77	0.26
OII4317	20	5	8.75	0.24
OII4319	20	5	8.76	0.25
OII4366	18	4	8.64	0.21
OII4414	33	3	8.78	0.10
OII4416	26	7	8.85	0.29
OII4641	27	5	8.74	0.20
OII4650	36	2	8.66	0.06
OII4661	18	3	8.72	0.16
OII4676	18	4	8.78	0.21
OII4069	37	3	8.86	0.09
OII4072	27	4	8.82	0.18
			$\epsilon_{\rm O}$ = **8.76**	$\Delta\epsilon_{\rm O}(\sigma)$ = 0.07
	$\Delta\xi_{\rm t}$(O) = 2.2		⇒	$\Delta\epsilon_{\rm O}(\xi_{\rm t})$ = 0.08

Table 18. Results from the abundance analysis of HD 35912 (B2 V).

HD 35912	$T_{\rm eff}$ = 18 500 K, log g = 4.0 dex			$\xi_{\rm t}$(Si)=3.2
Line	EW (mÅ)	ΔEW (mÅ)	$\epsilon_{\rm Si}$ (dex)	$\Delta\epsilon_{\rm Si}$ (dex)
SiII3856	65	2	7.35	0.05
SiII3862	62	4	7.53	0.11
SiII6347	99	2	7.60	0.03
SiII6371	71	3	7.49	0.06
SiIII4552	77	2	7.48	0.04
SiIII4567	60	2	7.45	0.05
SiIII4574	35	1	7.47	0.03
SiIII5739	30	2	7.51	0.07
			$\epsilon_{\rm Si}$ = **7.48**	$\Delta\epsilon_{\rm Si}(\sigma)$ = 0.07
	$\Delta\xi_{\rm t}$(Si) = 0.5		⇒	$\Delta\epsilon_{\rm Si}(\xi_{\rm t})$ = 0.04
HD 35912	$T_{\rm eff}$ = 18 500 K, log g = 4.0 dex			$\xi_{\rm t}$(O)=6.3
OII3945	15	5	8.88	0.32
OII3954	22	4	8.79	0.18
OII4317	25	5	8.82	0.20
OII4319	21	3	8.70	0.14
OII4366	22	5	8.70	0.23
OII4414	34	4	8.72	0.13
OII4416	29	3	8.85	0.11
OII4650	42	2	8.70	0.06
OII4661	25	3	8.86	0.13
OII4676	17	4	8.65	0.22
OII4069	44	3	8.91	0.08
OII4072	33	3	8.91	0.12
			$\epsilon_{\rm O}$ = **8.79**	$\Delta\epsilon_{\rm O}(\sigma)$ = 0.09
	$\Delta\xi_{\rm t}$(O) = 2.2		⇒	$\Delta\epsilon_{\rm O}(\xi_{\rm t})$ = 0.08

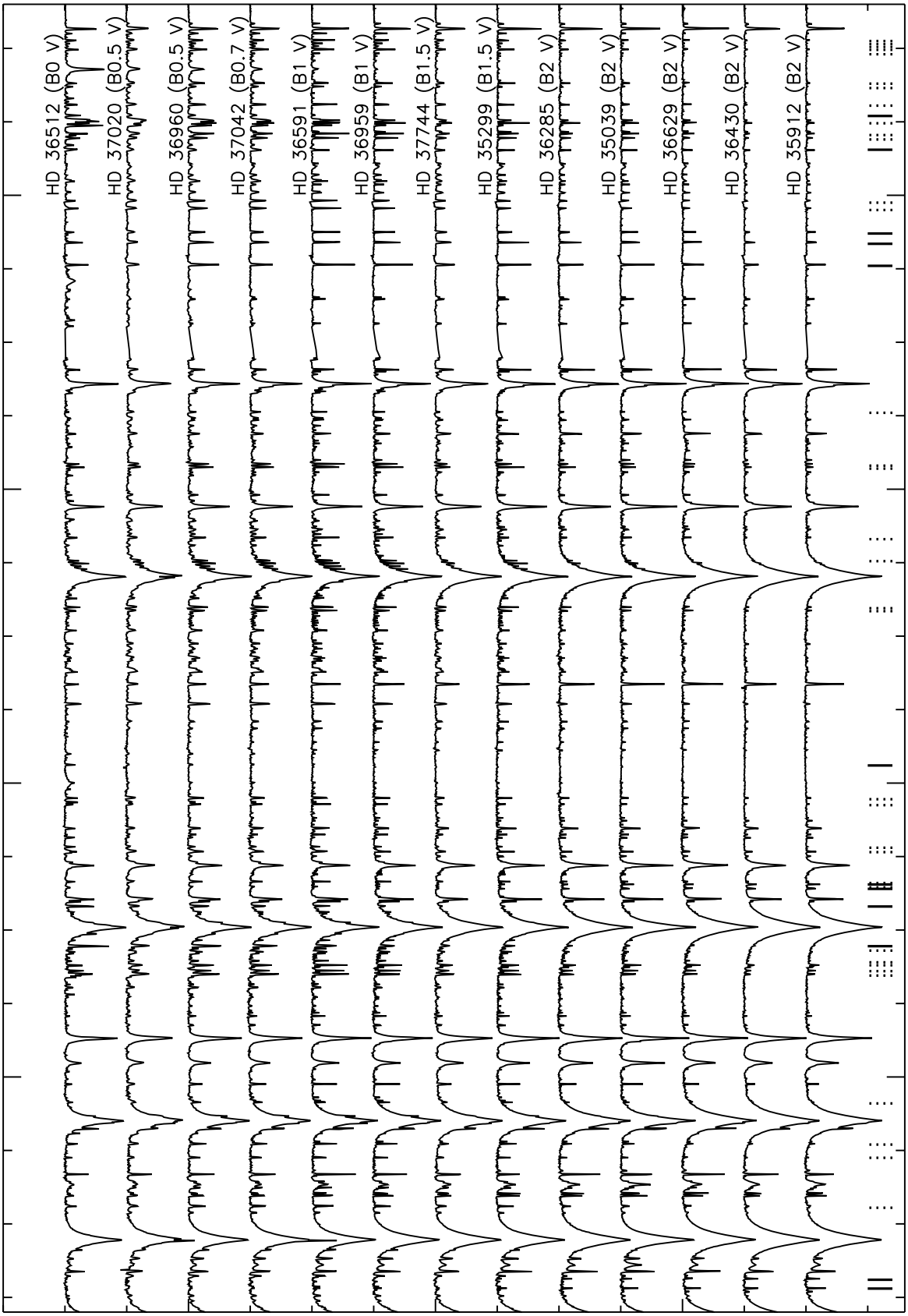

Fig. 8. The complete atlas of FIES@NOT spectra (part 1 of 3). The Si II-IV and O II lines used for the abundance analysis are indicated as solid and dashed vertical lines, respectively.

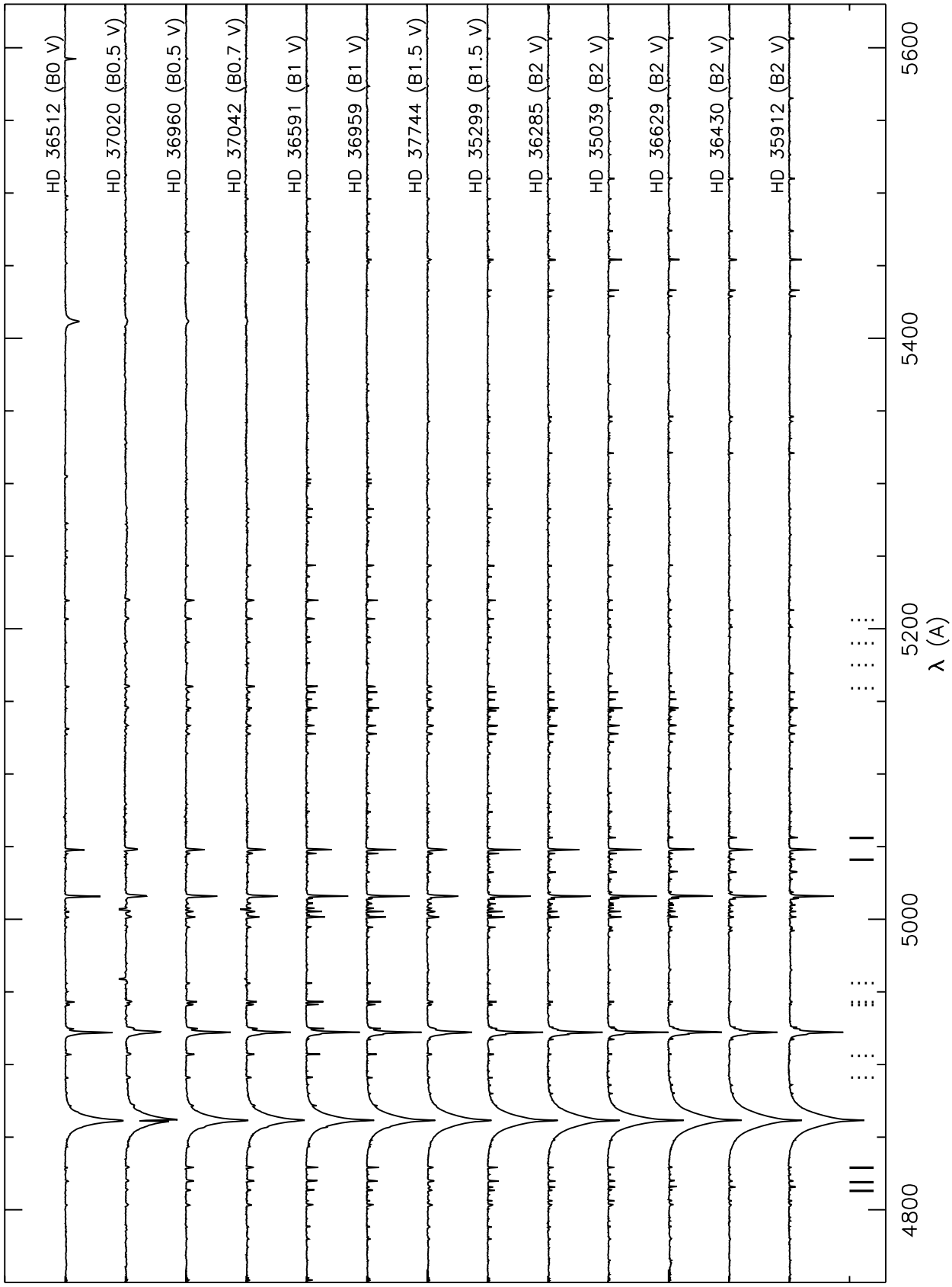

Fig. 8. continued.

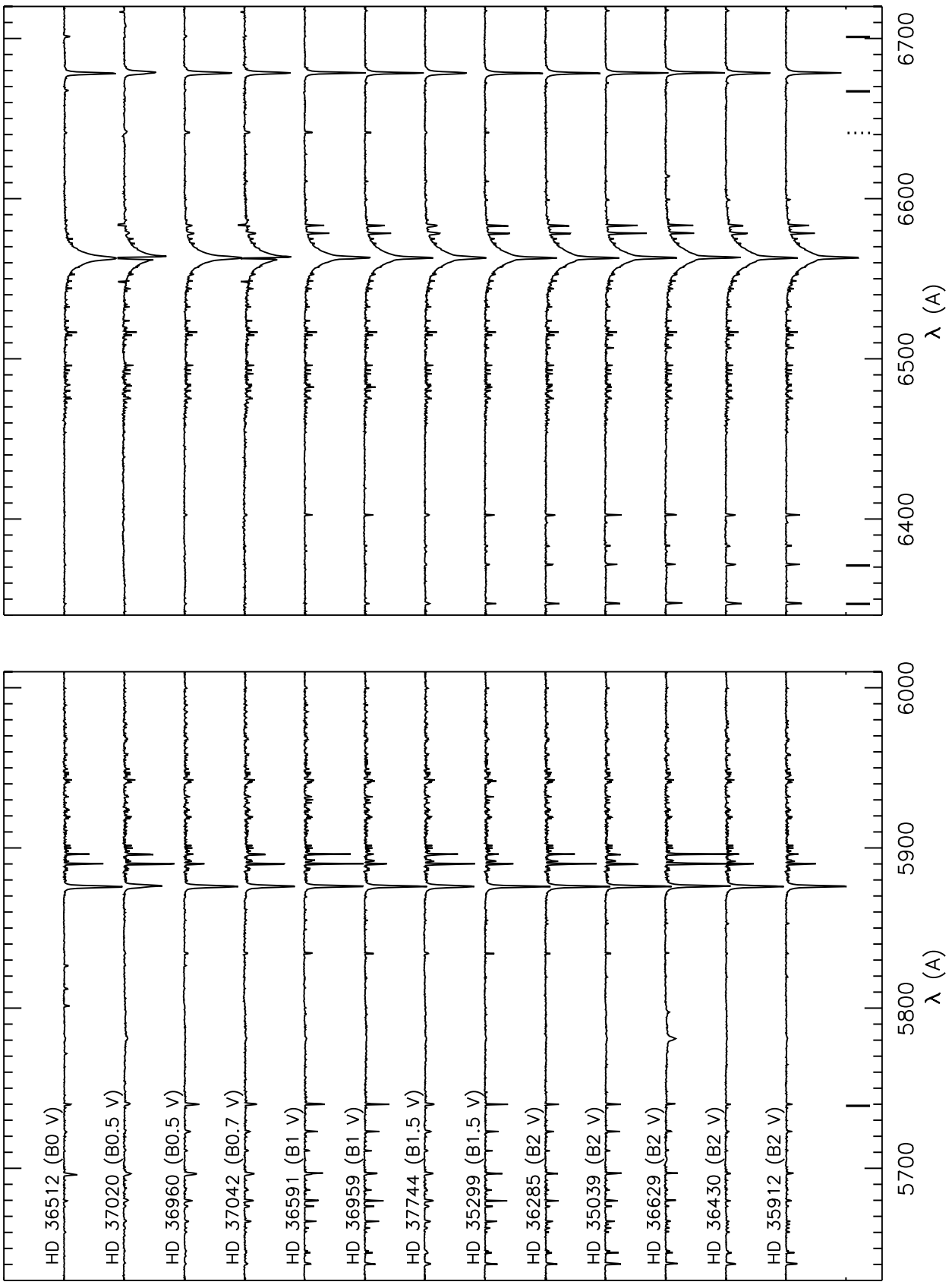

Fig. 8. continued.